Carbon Letters (2024) 34:565–601
https://doi.org/10.1007/s42823-023-00626-9

Online ISSN 2233-4998
Print ISSN 1976-4251

REVIEW

Preparation and properties of composite coatings, based on carbon nanotubes, for medical applications

Dorota Rogala-Wielgus[1] · **Andrzej Zieliński**[1]

Received: 9 January 2023 / Revised: 30 August 2023 / Accepted: 3 October 2023 / Published online: 16 November 2023

Abstract

The coatings based on carbon nanotubes (CNTs) are increasingly developed for their applications, among others, in medicine, in particular for implants in implantology, cardiology, and neurology. The present review paper aims at a detailed demonstration of different preparation methods for such coatings, their performance, and relationships between deposition parameters and microstructure and material, mechanical, physical, chemical, and biological properties. The thermal and electrostatic spraying, electrophoretic and electrocathodic deposition, and laser methods are presented. Characterization of microstructure of coatings, topography, morphology, adhesion of CNTs to a substrate, mechanical behavior, corrosion resistance, wettability, cytotoxicity, bioactivity, and antibacterial protection are reviewed for different deposition methods and parameters. The state-of-the-art in the field of carbon nanotubes shows a considerable number of research performed on CNTs coatings. The different forms of CNTs, deposition methods, parameters, and substrates were applied as process variables. The microstructures and surface homogeneity, chemical and phase compositions, mechanical properties at the micro- and nanoscale such as coating Young`s modulus and hardness, interface adhesion strength and delaminating force, open corrosion potential and corrosion current density, contact angle in wettability assessment, and bioactivity, cytotoxicity, and antibacterial efficiency among biological properties were determined. The summary of so far achievements, strengths and weaknesses, and important future research necessary for clarification of some weak points, development of non-toxic, mechanically and chemically resistant, bioactive, and antibacterial multicomponent coatings based on functionalized CNTs are proposed.

Keywords Carbon nanotubes · Coatings · Composites · Hardness · Young's modulus · Biological properties

Abbreviations

ACCVD	Alcohol catalytic chemical vapor deposition
AFM	Atomic force microscopy
Ag NPs	Silver nanoparticles
CA	Cellulose acetate
CFs	Carbon fibers
CGDS	Cold gas dynamic spray
CNTs	Carbon nanotubes
CS	Cold spraying
CVD	Chemical vapor deposition
DWCNTs	Double-wall carbon nanotubes
ECD or ECAD	Electrocathodic deposition, electroplating, electro-co-deposition
EPD	Electrophoretic deposition
ER	Endoplasmic reticulum
ES	Electrostatic spraying
FM	Fully melted
f-MWCNTs	Functionalized multi-walled carbon nanotubes
GO	Graphene oxide
HAp	Hydroxyapatite
HPCS	High-pressure cold spraying
HSLC	High-speed laser cladding
HUVECs	Human umbilical vein endothelial cells
HVOF	High-velocity oxygen fuel or oxy-fuel
IBAD	Ion beam-assisted deposition
LC	Laser cladding
LPCS	Low-pressure cold spraying
LVOF	Low-velocity oxy-fuel
MTT	3-(4,5-Dimethylthiazol-2-yl)-2,5-diphenyltetrazolium bromide

✉ Dorota Rogala-Wielgus
dorota.wielgus@pg.edu.pl

[1] Division of Biomaterials Technology, Institute of Manufacturing and Materials Technology, Faculty of Mechanical Engineering and Ship Technology, Gdansk University of Technology, 11/12 Narutowicza Str., 80-233 Gdańsk, Poland

MWCNTs	Multi-wall carbon nanotubes
nanoAg	Nanosilver
nanoCu	Nanocopper
nanoHAp	Nanohydroxyapatite
NEMS	Nanoelectromechanical system
PBF	Powder bed fusion
PCL	Polycaprolactone
PECVD	Plasma enhanced chemical vapor deposition
PEG	Poly(ethylene glycol)
PEO	Plasma electrolytic oxidation
PLA	Poly(lactic acid)
PLGA	Poly(lactide-*co*-glycolide)
PLLA	Poly(L-lactide)
PM	Partially melted
PMMA	Poly(methyl methacrylate)
PS	Plasma spraying
PU	Polyurethane
PVA	Polyvinyl alcohol
rGO	Reduced graphene oxide
ROS	Reactive oxygen species
SBF	Simulated body fluid
SHVOF	Suspension high-velocity oxy-fuel
SWCNTs	Single-wall carbon nanotubes
YSZ	Yttria-stabilized zirconia

1 Introduction

Recent medical implantology has utilized or investigated a huge number of materials in the form of solid implants or scaffolds, and also meshes, sponges, hydrogels, and coatings to modify the surfaces of metallic implants. Among them, the most recently, have appeared different forms of elementary carbon, principally single-wall or multi-wall carbon nanotubes (SWCNTs or MWCNTs of different chirality) but also carbon fibers (CFs), graphene, mainly as graphene oxide (GO) or reduced graphene oxide (rGO), fullerenes (especially C60) [1, 2]. The carbon nanotubes were discovered by Iijima [3]. Various types of synthesis techniques for CNTs include the arc-discharge method, laser ablation method, chemical vapor deposition (CVD), vapor-phase growth, flame synthesis method, and plasma-assisted growth [2].

All nanocarbon forms, particularly carbon nanotubes (CNTs), demonstrate extraordinary mechanical, thermal, magnetic, optical, electrical, surface, and chemical properties. Their electronic properties, high electric and thermal conductivity, and stiffness and strength are over those shown by any other material [4]. Thanks to these features, the CNTs have been frequently applied or recommended for use in different fields of the economy: medicine, biomechanics, energy storage, molecular electronics, fabrics and fibers, air and water filtration, and others [5].

As an additive to construction materials, they are presumably mostly applied as a component of epoxy resins. They have been used to improve the electrical and mechanical construction of epoxy-based composites [6–8]. They were given as fillers to strengthen several construction polymers [2, 9, 10] and also as functionally graded CNTs reinforced composites [11]. They can be considered components of bifunctional electrocatalysts [12].

As a component of coatings, they have been proposed to enhance heat transfer of heat sinks [13], improve corrosion performance [14–17], reinforce the coatings [18], increase the friction behavior [19, 20], make coatings superhydrophobic and usable for different applications [15, 21–23], such as the abrasion-resistant, photothermal, and anti-icing [24], and self-adapting ultra-high-temperature ceramic coatings [25]. The CNTs were used in coatings for electromagnetic interference shielding [26] and as a flame-retardant coating or composite material [27–29]. They were applied against decontamination of organic chemical pollutants in water [30, 31] and also involved in building space stealth and cosmic radiation shielding [32].

They are widely used in electronics and energy systems. Their electrical and electronic properties are suitable for building artificial muscles, electrochemical, thermal actuators, solvent and vapor actuators, fiber-shaped batteries and supercapacitors, color-changed electroluminescent and electrochromic fibers, mechanical and electrochemical sensors [33], thermal management systems [33, 34], solar cells [35], high-performance metal-ion batteries [36–38], energy storage and conversion devices [39], nanogenerators for harvesting energy [40], NEMS and hydrogen storage modules [2].

They are also increasingly developed for medical applications. They can be applied in bone regeneration, artificial neural conduits, and in drug and gene delivery in cancer therapy, brain therapy [41, 42], vaccine delivery [42], tissue engineering, and regenerative medicine, in particular for bone and muscle, and nervous system regeneration by neuronal differentiation and neuronal stimulation [42–45], for culturing the human embryonic stem cells and preserving their viability [46], and dosage forms and biomedical substrates in the pharmaceutical industry [47], They can be utilized in diagnosis for biomedical imaging, biosensors, for biomolecular detection and nanotweezers [42, 48]. They are introduced as sensors, in drug targeting, cancer diagnosis, and treatment, as antibacterial and antifungal species [49]. The CNTs helped to create the coatings releasing the active ingredients [50] such as biphosphonates, nucleic acids, proteins, and statins [51]. The integration of CNTs with polymeric scaffolds is promising for cardiac regeneration [52, 53]. The carbon nanotubes reinforced with chitosan, poly(lactic acid) (PLA), poly(lactide-*co*-glycolide) (PLGA), poly(ethylene glycol) (PEG), polyvinyl alcohol (PVA), and polycaprolactone (PCL) can mimic the extracellular matrices of bone [54]. These unique properties make CNTs promising candidates for cancer treatment and regenerative medicine, for bone, and nerve restoration [43, 55]. The incorporation of CNTs into polymer scaffolds results, among others, in increased scaffold strength and flexibility, improved biocompatibility, retardation of cancer cells` division, and enhancement of angiogenesis [1]. They are microbial and anti-adhesive [56–58]. They are used in various biosensors for biomolecular detection [59].

Besides the advantages, CNTs have two serious drawbacks. The first disadvantage important for medical applications is their anticipated toxicity which is a permanent feature of each nanoparticle; their small size and high surface area to volume ratio are associated with significant chemical reactivity, change in permeability and conductivity membranes of cells, lung penetration, and lung cancer risk [60]. The bioactivity and cytotoxicity of CNTs are affected by their diameter, length, and functionalization in vitro and in vivo, as well as by the fabrication method with nickel catalyst [61] and may make CNTs toxic for living organisms or the environment [60, 62]. The toxicity can manifest itself as membrane damage, DNA damage, an appearance of oxidative stress, and changes in mitochondrial activity and intracellular metabolic routes as a consequence of the highly hydrophobic surface and the non-biodegradable nature of the CNTs [1]. However, the CNTs are considered to have carcinogenicity mainly to enhance lung tumors, and the carcinogenicity may attenuate with decreasing tube length [63]. The MWCNTs are likely to be a more neural-friendly interface than SWCNTs since they allow for a wider external surface and effective functionalization [64].

The second disadvantage is the weak adhesion of CNTs (and all carbon nanoforms) to any material. It is critical to functionalize CNTs not only to make them more soluble, but also to allow their integration into many organic, inorganic, and biological systems and applications, and eliminate or at least minimize their toxicity. A proper functionalization of the CNTs is nowadays carried out by a variety of methods [65–68]. It may follow two strategies: (1) chemical reactions occurring at the sidewalls and tips of CNTs and (2) oxidation followed by an appearance of carboxyl-based bonding [41]. Functionalization of carbon nanofibers can be performed by CVD and plating of some compounds, and by chemical or biochemical reactions [69].

This review aims to show the newest data on carbon nanotubes creating coatings or being components of such, in particular (1) various synthesis methods, in particular the electrophoretic deposition (EPD) technique as the most preferred, (2) their properties, such as surface morphology and topography, mechanical, corrosion, and biological properties, and the relationships between output and input variables to optimize the deposition process.

2 Forms of carbon nanotubes

Carbon nanotubes are hollow structures created from rotating a graphene layer around one axis in a certain direction. It is an sp^2 form of hybridization of carbon derive, where carbon atoms are organized with strong covalent bonds in

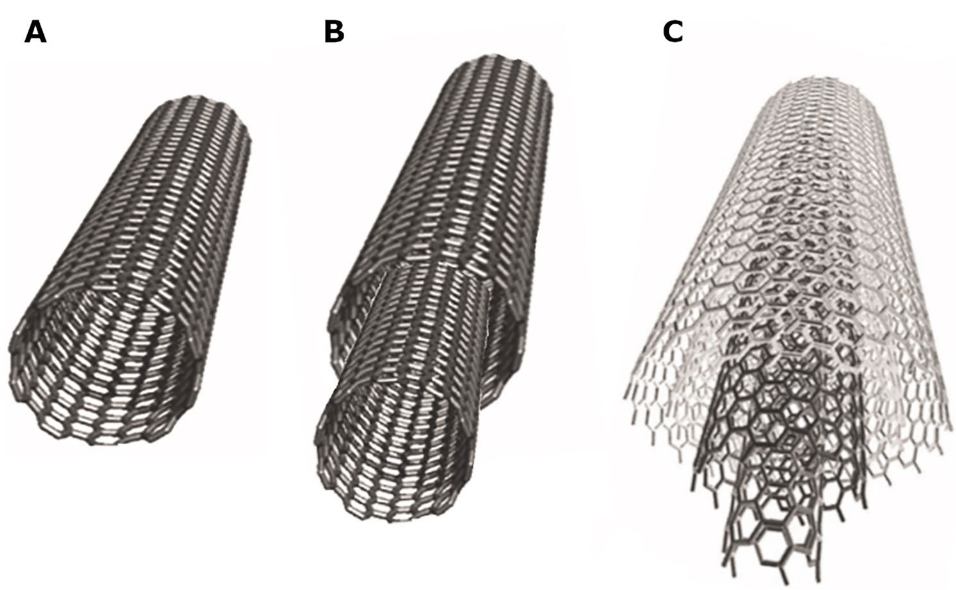

Fig. 1 CNTs types based on a number of walls, where **A** SWCNTs, **B** DWCNTs, and **C** MWCNTs. Figures **A** and **C** were reproduced with permission [74] Copyright 2011, InTech

a hexagonal lattice, very similar to graphene, graphite, and fullerenes. Carbon nanotubes can be divided into SWCNTs, double-wall carbon nanotubes (DWCNTs), and MWCNTs [70], which are demonstrated in Fig. 1. The first reported were MWCNTs by Iijima [3]. MWCNTs are composed of concentric cylinders with regular periodic interlayer spacing located around the ordinary central hollow. They form a layer construction with van der Waals bonding between cylinders [71–73].

Literature shows that the parameters of all types of carbon nanotubes are within certain limits as illustrated in Tables 1 and 2.

Besides the division grounding on the number of carbon nanotube walls, some SWCNTs forms differ in terms of wrapping to a cylinder structure, such as armchair (integers $n=m$), zigzag (integers $m=0$), and chiral (other integers) [72]. Figure 2 illustrates schematic types of wrapping graphite sheet to form different forms of SWCNTs.

There are several methods of synthesis of carbon nanotubes such as chemical vapor deposition, arc-discharge method, laser ablation method, spray pyrolysis, hydrothermal methods, and thermal plasma [48, 70, 85–87].

Table 1 The physical properties of three types of CNTs

Property	MWCNTs	DWCNTs	SWCNTs
Interlayer spacing	0.34÷0.39 nm [72]	0.33÷0.42 nm [75]	–
Inner diameter	4÷7 nm [76]	1÷3 nm [2]	–
Outer diameter	2÷30 nm [72]	2÷4 nm [2]	0.4÷3 nm [72, 77]
	15÷25 nm [76]		Made with CVD 1.3÷1.5 nm [78]
Length	Up to 50 µm [76]	100÷475 nm [79]	CVD 13 µm [78]
	100 nm÷1 cm [77]	100 nm÷1 cm [77]	CVD 140 nm÷3200 nm [80]
Ends	Closed and capped with half-fullerene molecules [72]	Capped and open-ended [81]	Can come together and form bundles [72]

Table 2 The mechanical properties of three types of CNTs

Property	MWCNTs	DWCNTs	SWCNTs
Young's modulus	1.7÷2.4 TPa [83]	0.33÷0.42 TPa [75]	2.8÷3.6 TPa [83]
Tensile strength	63 GPa [77]	77.51÷157.5 GPa[a] [84]	53 GPa [77]

[a]Predicted based on finite element method and chirality

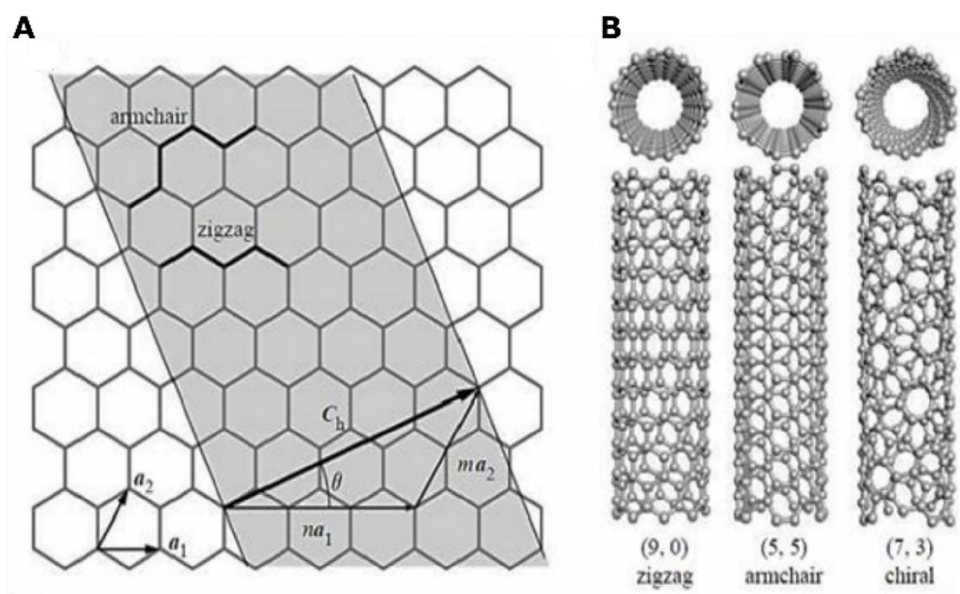

Fig. 2 A scheme illustrating **A** forms of wrapping graphite to achieve different structures of the SWCNTs and **B** different structures of SWCNTs based on the chiral angle. The figure is reproduced with permission [82] Copyright 2016, JACS Directory©2016

3 CNTs-containing coating types and their deposition methods

There are many types of CNT-included coatings, with ceramics, metals, polymers, or mixed. Examples of such coatings are shown in Fig. 3. Several deposition methods of CNTs-containing coatings, like the main groups: thermal spray, electrochemical deposition, and laser methods, are schematically shown in Fig. 7. The main advantages and disadvantages of the types of deposition methods are listed in Table 3. The examples of CNTs-containing coatings and their main parameters of synthesis with described impact on coatings properties are listed in Tables 4 and 5.

3.1 Thermal spraying

A thermal spray is a group of processes in which materials (metals, alloys, metal oxides, metal/ceramic blends, carbides, composite materials) are deposited using spraying. The processes differ from each other basically by the state of the material: molten, semi-molten, or solid state. The thermal spraying method is used in many fields in mechanical engineering, for corrosion protection, surface restoration, and repair, heat insulation or conduction; energy technology, and biomedical and industrial areas [88, 89]. Apart from many advantages, the technique has also some drawbacks. Covering parts with complex shapes, inner surfaces, and narrow parts is limited. Some advances in thermal spray technology enable covering a such surface, named the internal diameter thermal spray method [90, 91]. Figure 4 shows a schematic illustration of literature-based three most used methods of CNTs deposition techniques.

3.1.1 Plasma spraying

Plasma spraying (PS) is one of the thermal processes used to coat materials. This method uses a high-energy heat source, which melts (at a temperature of about 10,000 K) coating material inserted into a plasma jet and sprayed onto a prepared substrate [92–94]. The arc between two electrodes cathode (tungsten) and anode (copper) is initiated by high-frequency discharge in the presence of gases, such as Ar, He, H_2 and N_2 named plasma-forming gases [93, 94]. Figure 4 A shows a schematic illustration of the PS coating method.

3.1.2 Cold spraying

Cold spraying (CS) or cold gas dynamic spray (CGDS) is not only a thermal spraying process but also a solid-state spraying method. It differs from other thermal spraying methods by the state of powder feedstock, which is always unmelted. This method is used to produce metallic and metallic-ceramic coatings. Based on pressure level, the cold spraying process (Fig. 4C) can be divided into low-pressure cold spraying (LPCS) and high-pressure cold spraying (HPCS). This process is based on the acceleration of particles of the coating material by pressurized gas (air, N_2, He, or mixture) in a diverging-converging nozzle, leading to preparation layer-by-layer [89, 95] coating. The best adhesion of the cold-sprayed coatings is achieved only above a critical particle velocity [96].

3.1.3 High-velocity oxy-fuel thermal spraying

High-velocity oxygen fuel (HVOF) is a thermal spray technique that uses fuel, such as H_2, propylene, acetylene, or kerosene to achieve a high temperature that ranges from 2500 to 3000 °C and high pressure in the combustion chamber. Most commonly a powder, but also a suspension (another type of HVOF, named suspension high-velocity oxy-fuel SHVOF) is inserted in the nozzle and at the same time heated and accelerated (particle velocity of 550–1060 m/s) by a gas stream causing the formation of a relatively dense coating, with good adhesion properties. Coatings deposited by the HVOF method (Fig. 4 B) are widely used to enhance surface performance and protect against corrosion and wear, but it also is a convenient method to deposit nanomaterials [91, 97–100]

Fig. 3 Scheme of types of carbon nanotube coatings

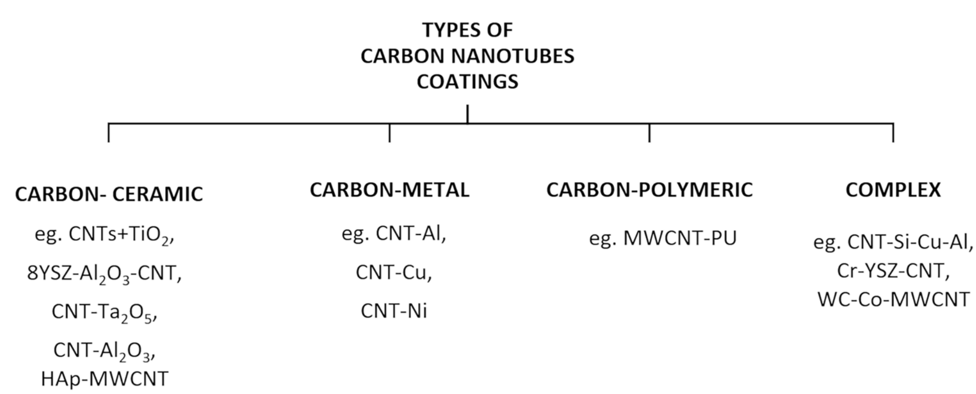

Table 3 The main advantages and disadvantages of CNTs coating deposition techniques

The main group of a coating deposition method	Type of a coating deposition method	Advantages	Disadvantages	Reference
Thermal spraying	PS	Ability to coat a wide range of materials (a high-heat source, temperature ranging from 3000 to 25,000 °C), low thermal impact on working surfaces, high particle velocity in the range of 240–610 m/s, ability to change parameters according to the required effect (flame temperature, particle velocities, particle size distribution), comprehensive performance at a good level	Risk of CNTs structure deformation, due to high temperature in some cases was observed, regions with semi-molten material in the coating, generating defects, such as pores and cracks, the high temperature causes the substrate surface to (low level) melt during the PS process the coating material is molten during the PS process, the temperature and particle velocities in function with the distance between torch and substrate are crucial parameters to determine the appropriate coating microstructure, properties, and efficiency of the process, the deposition angle to the substrate has an impact on the microstructure and properties of the deposited coating, oxidation appears during the PS process, minimalized by using a vacuum chamber	[31, 88, 93, 94, 98]
	CS	High particle velocities in the range of 300–1200 m/s, sprayed material doesn't melt during the deposition process, the pureness of achieved coatings, the substrate maintains its properties due to low heat input, high-quality coatings, a wide range of coating materials, complex shape materials might be coated, minimal effects of oxidation, decomposition, grain growth, and phase change	High-pressure requirement, lower size distribution of the powders than in HVOF	[88, 107, 108]
	HVOF	The substrate maintains its properties due to low heat input (less than 150 °C), wide range of coating compositions, very high particle velocities of 550–1060 m/s (coatings with higher densities, smoother, lower oxide levels than in other thermal spraying methods with lower particle velocities), is used to prepare corrosion and wear-resistant coatings	The deposition angle to the substrate has an impact on the microstructure and properties of the deposited coating, less sensitive to the distance between the nozzle and substrate than the PS method, oxides with a higher melting point may be difficult to melt and thus to coat	[88, 98]
	LVOF	The substrate maintains its properties due to low heat input (lower than in HVOF), the particle velocities are higher than in the conventional PS method, improving coatings properties (level of oxides, density, surface topography), is used to prepare corrosion and wear-resistant coatings	Lower particle velocities than HVOF, give coatings with lower densities and higher oxide levels, the deposition angle to the substrate has an impact on the microstructure and properties of the deposited coating	[88, 98]

Table 3 (continued)

The main group of a coating deposition method	Type of a coating deposition method	Advantages	Disadvantages	Reference
Electrochemical methods	ES	Simplicity, low cost, time-saving, ability to achieve thin films, ability to deposit coatings with different morphologies, without vacuum requirement, sub-micrometer or nanoscale droplets of deposition material, self-dispersive and high-wettability droplets of deposition material, huge variety of compatible substrates, a large variety of coating materials, high deposition efficiencies due to charged droplets, and thus reduced material consumption, high coatings quality, low substrate temperatures, uniform distribution of CNTs in the polymer matrix (ex. PU)	The ES nozzle tip might be clogged when depositing graphene nanosheets, an additional annealing is required to obtain a particular crystalline phase	[103, 109, 110]
	EPD	A low-cost method, simplicity, ability to coat different shapes, a wide range of coating materials, low coating time and temperature, adjustable parameters of EPD, enabling control of deposit thickness and thus its parameters, uniformity of achieved coatings, a microstructural homogeneity of the coatings, a purity of deposited materials, the use of alternating current electric fields elongate nanoparticles, which align uniformly and orientate themselves along the electric field direction, thus enabling manipulation of the coating material deposition	The use of water as a solution to EPD bath may cause hydrolysis, thus bubble formation in the coating, the Joule heating appears when excessive voltage is applied, the use of lower voltages than the voltage of water electrolysis, causes deposited coatings to be of poor quality, an additional annealing might be required to obtain a particular crystalline phase or to improve coating quality	[111–117]
	ECD	Adjustable parameters of the ECD, thus control over deposit parameters, a low-cost method, simplicity, a wide range of coating materials, a purity of deposited materials, ability to coat different shapes	The method generates an excessive amount of sludge, to recover metals from suspension is problematic, the long-term impact of sludge disposal on the environment	[117, 118]
Laser methods	HSLC	The coating is uniform, higher melting speed than in the LC process, the coating might be thinner than in the LC process, ability to deposit smooth coatings, the cooling rate is higher than in the LC process, the deposited coatings are almost without defects, such as pores, or cracks, a wide range of coating materials, more limited heat-affect zone than in the LC, minimum dilution, small stress deformation, good metallurgical bonding	The substrate is melted during the HSLC process, the coating material is melted while deposited	[119–121]
	LC	High-flexibility deposition parameters, a rapid solidification of the deposit, wide range of coating materials, limited heat-affect zone, minimum dilution, small stress deformation, good metallurgical bonding	The substrate is melted during the LC process, the coating material is melted while deposited, lower melting speed than in HSLC, lower cooling rate than in HSLC	[121, 122]

Table 4 Examples of CNTs coating combinations and the parameters of synthesis

Coating	Substrate	Method	Main parameters	Coating specification	References
CNT–Al–Si	Mild steel	PS	A thoriated tungsten cathode; a concentric copper anode; the plasma power ~ 22 kW; the gun traverse velocity was 25 mm/s; a distance between a substrate and gun (standoff distance): 100 mm	Structure: two-phase microstructure composed of Al–Si matrix with uniformly distributed CNTs, and CNTs clusters, showing strengthening effect by fiber pull-out and crack bridging. The porosity of the coating is in the range of 10–12% Properties: the addition of CNTs in the concentration of 5 wt% and 10 wt% of CNTs to Al–Si coating improved the elastic modulus in the nanoindentation test of 19% and 39% respectively (with no difference in micro-scale compression test), the yield strength of 17.5% and 27%, respectively (in micro-scale compression test 27% and 77% respectively), and elastic recovery properties. Also, the wear volume in the nano-scratch test was decreased for the concentration of 5 wt% and 10 wt% of CNTs by 34% and 71% respectively, and in the macro-scale wear test was respectively decreased by 68% and increased by 15%. The nanoindentation elastic modulus for the 5 wt% and 10 wt% of CNTs in the coating was reported at 107 ± 6 GPa and 125 ± 7 GPa, respectively, and in the micro-scale of 4.95 ± 0.05 GPa and 5.65 ± 0.95 GPa, respectively	[123, 124]
TiO_2–CNTs	AISI 4140	PS	The working gas: a mixture of Ar (primary gas, 42 L/min) and H_2 (secondary gas, 10 L/min); the spraying voltage: 72 V; the spraying current: 550 A; the spraying distance: 80 mm	Structure: nanostructure coating, consisting of the following regions: fully melted (FM), and partially melted (PM) with solid elements and pores. The CNTs structure is destroyed due to the PS process. In some regions TiO_2 and C formed chemical bonding and in some physical Properties: the addition of CNTs to TiO_2 coating has a strengthening effect thus, the scratch resistance of the TiO_2–CNTs coating in comparison to TiO_2 coating was enhanced by around 38.6% and lubricating effect reduced the lateral friction force	[94]

Table 4 (continued)

Coating	Substrate	Method	Main parameters	Coating specification	References
MWCNTS–YSZ (yttria-stabilized zirconia)	INCONEL 738	Plasma thermal spray	Ionization of argon	Structure: a porosity and microcracks were distinguished Properties: the concentration of 8 wt% of CNTs improved the best hot corrosion resistance (at 950°C) of YSZ material (the weight change was of 0.0057 mg/cm^2), while the weight change for bare YSZ was 1.1 mg/cm^2, thus all coatings with the addition of CNTs exhibited improvement in hot corrosion resistance of the YSZ	[125]
CNTs	ADC12 Al alloy	Plasma electrolytic oxidation (PEO)	The voltage: 400 V; the pulse frequency: 400 Hz; the positive duty cycle: 35%; the negative duty cycle: 20%; the positive and negative pulse ratio: 1:1; the oxidation time was: 20 min, the anode: a substrate; the cathode: stainless steel; the temperature of the electrolyte: <35 °C	Structure: the regulation of coating microstructure by the addition of CNTs. Porosity was observed Properties: the CNT-dopped PEO coatings improve the corrosion resistance of the ADC12 Al alloy (especially with a concentration of 1.5 g/L of the CNTs) by sealing pores. Also, the addition of CNTs improves thermal conductivity	[126]
Zirconia–alumina–CNT	P91 steel	PS	The gun: F-4 plasma gun; the plasma current: 500 A; the plasma voltage: 66 V; the primary gas argon flow: 38.5 nlpm[a]; the secondary gas hydrogen flow: 4 nlpm[a]; the carrier gas nitrogen flow: 3.30/4.25 L/min; the powder feed rate: 40 g/min; the spray distance: 120 mm The traverse speed: 0.0011 m/s	Structure: the CNTs are well dispersed in the zirconia-alumina matrix. The CNTs remained undamaged, despite high temperature during the PS process. Porosity was observed, while the CNTs addition reduced it (3 wt% of CNTs reduce coating porosity by 70%) Properties: the addition of CNTs increases thermal conductivity (from approximately 0.4 W/mK for base coating to 0.9 W/mK for coating with CNTs), microhardness, and corrosion resistance in contrary to the base alumina-reinforced coating	[127]
TiO_2/CNTs		PS	The argon flow rate: 80 L/min; the argon pressure: 0.69 MPa; the hydrogen flow rate: 15 L/min; the hydrogen pressure: 350 kPa; the arc current: 500 A; the arc voltage: 65/75 V; the powder feed rate: 40 g/min; the spray distance: 10 cm	Structure: the coating has low porosity and it doesn't change with the addition of CNTs Properties: the composite coating exhibited higher photocatalytic activities than the base TiO_2 coating, with the concentration of methylene blue solution decreased by approximately 35%	[128]

Table 4 (continued)

Coating	Substrate	Method	Main parameters	Coating specification	References
CNT-doped Ta_2O_5	Ti6Al4V alloy	Atmospheric-PS	The arc voltage: 70 V; the arc current: 500, 550, 600, 650 A; the primary plasma gas Ar: 50 L/min; the secondary plasma gas H_2: 12 L/min; the carrier gas Ar: 3 L/min; the powder feed rate: 40 g/min; the spray distance: 100 mm	Structure: the addition of CNTs increases the coating porosity Properties: the addition of CNTs doesn't impact coating roughness and reduces microhardness, while the increased concentration of CNTs increases elastic modulus and indentation fracture toughness. Also, the biological tests were conducted and showed excellent osteoblast-like osteosarcoma MG-63 cell adhesion and viability after 7 days of incubation	[31]
Al_2O_3–TiO_2–MWCNTs	Mild steel (C45 grade)	Air-PS	The plasma gun: 3 MB; the arc current: 490 A; the arc voltage: 70 V; the powder feed: 50 g/min; the argon flow rate: 33/38 L/min; the hydrogen flow rate: 7.1 L/min; the spray distance: 127 mm	Structure: the CNTs are well dispersed in the Al_2O_3–TiO_2 matrix, without damage that might appear due to high temperatures during the PS process. The addition of CNTs and their increased concentration decreases the porosity of the coating Properties: the addition of CNTs increases the adhesion strength and roughness of the coating and alumina alpha phase the resistance to high temperature	[129]
CNT–Al	AZ91 Mg alloy	CS + PEO	CS: the carrier gases: nitrogen; the gas pressure: 1.7 MPa; the gas temperature: 350 °C; the gun travel speed: 200 and 80 mm/s; the feeding rate: 2.7 g/mm; the standoff distance: 30 mm PEO: the pulsed power: 15 kW; the current combination of 0.3 and 0.6 A; the pulse frequency: 2000 Hz; the duty cycle: 20%; the oxidation time was: 10 min	Structure: good contact with base material without cracks but the roughness of PEO threated CNTs coating was higher Properties: the hardness and elastic modulus of the coating were 13.9 GPa and 185.4 GPa, respectively, and demonstrated almost the same corrosion resistance as the basic CS coating. The coating also showed a 59.8% lower wear rate and 15.6% lower friction coefficient than the CS coating	[107]
CNT–Al	AZ91 Mg alloy	CS	The carrier gases: nitrogen; the gas pressure: 1.7 MPa; the gas temperature: 350 °C; the gun travel speed: 200 and 80 mm/s; the feeding rate: 2.7 g/mm; the standoff distance: 30 mm	Structure: the coating has lower porosity than the Al coating Properties: the hardness and elastic modulus of the coating were 1.66 GPa and 77.6 GPa, respectively, and demonstrated higher corrosion and wear resistance than Al coating	[130]

Table 4 (continued)

Coating	Substrate	Method	Main parameters	Coating specification	References
CNT–Cu	Cu plate	CS	The carrier gases: nitrogen; the gas pressure: 3.2 and 2.8 MPa; the gas temperature: 200 and 500 °C; The gun travel speed: 10 mm/s; the feeding rate: 5.65 cm^3/min; the standoff distance: 35 mm	Structure: the 5 vol.% of CNTs coating demonstrated well-fused CNTs. Higher volume concentrations of CNTs showed noticeable particle interfaces Properties: the maximum heat transfer coefficient of the coatings was 1.21–1.74 times improved contrary to the plain Cu plate. The best-boiling heat transfer performance thus lowering the superheat and improving the heat transfer coefficient was achieved for the one-layer coating with 15 vol.% CNT	[131]
Cu–CNT–AlN Cu–CNT	Cu plate	CS	The carrier gases: nitrogen; the gas pressure: 3.2 and 2.8 MPa; the gas temperature: 200 and 500 °C; the gun travel speed: 25 mm/s; the feeding rate: 24.80 and 21.95 g/min; the standoff distance: 35 mm	Structure: the swerve particle deformation and lamellar structure, porous surface, and dense internal microstructure [132] Properties: the as-prepared coatings are more wettable in liquid R134a. The Cu–CNT coating exhibited a maximum boiling heat transfer enhancement ratio of 1.48. The heat transfer of the Cu–CNT decreased at high heat fluxes, where maximum improvement was observed at heat fluxes within 100–200 kW/m^2	[132, 133]
CNT–AlSi	Stainless steel	CS	The carrier gases: nitrogen; the gas pressure: 3.0 MPa; the gas temperature: 500 °C; the gun travel speed: 100 mm/s; the nozzle traverse speed: 500 mm/s; the standoff distance: 30 mm	Structure: microlaminated structure, containing fine grains, without damage to the CNTs structure and interfacial reaction between Al and CNTs	[108]
Nickel-plated CNTs/FeCoNbBSi	45-steel shaft	HSLC	The laser power: 2400 W The laser feed rate: 1 mm/s; the powder feed rate: 40 g/min; the gas flow: 10 m/min; the powder-defocusing amount: 13 mm; the laser defocusing amount: 9 mm	Structure: refined structure with an increase of Ni-plated CNTs Properties: with the increased concentration of Ni-plated CNTs the friction coefficient decreased and wear and corrosion resistance increased	[119]

Table 4 (continued)

Coating	Substrate	Method	Main parameters	Coating specification	References
Ti–MWCNT	Titanium	LC	The laser power: 700 W; the spot size: 2 mm; the scanning speed: 5 mm/s; the gas flow rate: 20 L/min	Structure: the increasing concentration of CNTs in the coatings caused TiC grain size enlargement Properties: the addition of the CNTs improved high-temperature corrosion resistance and lowered friction coefficient contrary to the Ti substrate	[120]
Al_3Ti–Cu–SiC–CNTs	TA2 titanium alloy	LC	The laser power: 800/1200 W, the laser beam diameter: 4 mm, the powder feeding rate: 20/30 g/min, the laser scanning speed: 2/8 mm/s, the gas flow rate: 30 L/min	Structure: the microstructure showed a large amount of point defects Properties: the addition of the CNTs decreased the friction coefficient	[134]
Ni–WC–CNT	Stainless steel	LC	The spot diameter: 4 mm; the laser power: 1000 W; the scanning velocity: 240 mm/min; the gas flow rate: 25 g/min	Structure: the addition of CNTs caused refined grains in the coating material Properties: the coatings with a concentration of 3 wt% of CNTs exhibit the highest microhardness and wear resistance	[122]
MWCNT/PU	Q235 steel	ES	The pressure of compressed air: 0.4÷0.7 MPa; the voltage: 50–60 kV; the distance between the spray gun and specimen: 100÷150 mm; the sintering temperature: 220 °C; the sintering time: 30 min	Structure: the MWCNTs were uniformly distributed in the PU matrix, forming a network structure Properties: the addition of MWCNTs to PU matrix enhanced the thermal conductivity of the coating and the corrosion resistance of the steel ground grid	[110]
Cu–CNT–TiO_2	Cooper tubes	ES	The electrostatic material: 2 wt% polyvinyl alcohol (PVA) solution; the sintering temperature: 350 °C; the sintering rate: 20 °C/min	Structure: porous structure Properties: the wettability of the coating (12.85°) is higher than the substrate material and also coating heat transfer is improved in comparison to the cooper tubes	[135]
CNT–CNP CNT–CNP–TiN	Al	High-voltage ES	The distance between the needle and substrate: 30 mm; the applied voltage: 9 kV; the spraying amount for each coating: 35 µL; the coatings drying temperature: 110 °C; the coatings drying time: 30 min	Structure: micron-sized porosity observed Properties: the addition of CNTs mesh into the structure improves light absorption properties	[103]

Table 4 (continued)

Coating	Substrate	Method	Main parameters	Coating specification	References
Cr–YSZ–CNT	Steel plate	ECD	The cathode: a substrate; the anode: graphite; the duration: 180 min; the current density: 400 mA/cm^2; the pH: 1.5; the temperature: 20 and 25 °C	Structure: well-dispersed CNTs in a matrix and cauliflower-like structure of the Cr–CNT coating. The coatings were almost free from microcracks and pores Properties: the addition of CNTs lowers friction coefficient and reduces wear rate in contrary to Cr and Cr–YSZ. The Cr–YSZ–CNT coating exhibited a hardness of 24 GPa and the lowest surface roughness of 0.22 µm according to Cr and Cr–YSZ coatings	[136]
Cr–YSZ–CNT	Steel plate	ECD	The cathode: a substrate; the anode: graphite; the duration: 120 min; the current density: 400 mA/cm^2; the pH: 1.5; the temperature: 20÷25 °C	Structure: dense and uniform coatings with reduced cracks appearance Properties: the coating exhibited a hardness of 25 GPa and elastic modulus of 206 GPa, and enhanced wear resistance in comparison to coatings without CNTs. The CNTs exhibited lubricating and bridging properties	[137]
Ni–CNT	Steel	ECD	The cathode: Ni plate; the anode: a substrate; the current density: 5 A/dm^2; the temperature: 50 °C; the ultrasonic agitation: 42 kHz, 30 W; the vibration frequency: 42 kHz; a bath consists of nickel sulphonate and CNTs	Structure: the CNTs were well dispersed and embedded in Ni-matrix Properties: the Vickers hardness of the Ni–CNTs coating exceeds 500 HV (for the concentration of CNTs of 1 g/L). The bonding strength of CNTs to Ni was 1.3 times improved by using the ECD technique, thus eightfold elongating tool life. The surface roughness of Ni–CNT coating was 0.28 µm	[138]
Fe–Cr–CNTs	Mild steel	LVOF	The C_2H_2 flow rate: 25.95 L/min; the C_2H_2 pressure: 0.1 MPa; the O_2 flow rate: 21.23 L/min; the O_2 pressure: 0.24 MPa; the N_2 flow rate: 33.03 L/min; the N_2 pressure: 0.72 MPa; the spray distance: 200 mm; The spray rate: 108 g/min	Structure: the homogenous and uniformly distributed CNTs in the coating Properties: the ID/IG ratio was less than 1, showing a low range of structural defects in CNTs coating, making the LVOF technique an excellent candidate for CNTs coatings deposition method	[102]

Table 4 (continued)

Coating	Substrate	Method	Main parameters	Coating specification	References
WC–Co–MWCNTs	AISI 416 stainless steel discs	HVOF	The combustion chamber pressure: 6–8 bar; a rotating substrate	Structure: the porosity was decreased in contrary to coating without MWCNTs Properties: the addition of CNTs caused the decreased microhardness and increased fracture toughness, and also the reduction of friction coefficient at high power conditions (improved wear performance). In medium and lower power the result was inverse	[90]
WC–Co–CNTs	Mild steel of AISI 1020	HVOF	The flow rate of O_2: 900÷950 L/min; the kerosene flow rate: 0.38 L/min; the gas (Ar) flow rate: 50÷60 L/min; the torch velocity: 700 mm/min; the powder feed rate: 70÷75 g/min; the spray distance: 200–250 mm	Structure: the porosity was reduced due to the addition of CNTs, which were well dispersed and adhered Properties: the addition of CNTs increased microhardness, reduced roughness, lower friction coefficient, and improved wear resistance	[97]
Ni–Cr/CNTs	Mild steel	HVOF	The C_3H_8 flow rate: 65.73 L/min; the C_3H_8 pressure: 0.97 MPa; the O_2 flow rate: 238.5 L/min; the O_2 pressure: 1.21 MPa; the air flow rate: 201.3 L/min; the air pressure: 0.9 MPa; the spray distance: 280 mm; the spray rate: 110 g/min	Structure: the porosity of the coating was in the range of 0.49–1.01 vol.%. The CNTs in the coating were well bonded Properties: the addition of CNTs 20% increased the Vickers hardness and improved wear and corrosion resistance	[139]

[a]Normal liter per minute; L/min, a unit of the volumetric flow rate of a gas at standard conditions for temperature and pressure

Table 5 Exemplary parameters of electrophoretically deposited CNTs coatings

Coating	Substrate	Main parameters	Coating specification	References
MWCNTs	Ti13Zr13Nb	The EPD voltage: 20 V; the EPD time: 0.5 min; the anode "+": substrate; the cathode "−": platinum; the content of MWCNTs: 0.19 wt%	Properties: The MWCNTs coatings were laser modified. It was reported the laser modification caused a lack of surface cracks. The contact angles of examined surfaces were in the range of 46°–82°, the hardness from 4.51 to 6. 36 GPa (higher for laser-melted layers than affected by the heat of the laser beam), and Young's modulus from 105.28 to 125.19 GPa (lower for laser-melted layers than affected by the heat of the laser beam)	[112]
CNTs	Ti pure	The EPD voltage: 28 V; the EPD time: 30 s; the EPD current range 6–13 mA; the anode "+": substrate; the cathode "−": no data; the content of CNTs: no data	Properties: The human osteoblasts NHOst cell viability was slightly increased after 7 days of incubation by the surface modification of Ti alloy with MWCNTs coating. The hardness of the coating was 1.664 ± 0.107 GPa (132 ± 37 HV), Young's modulus of 101 ± 15 GPa, and corrosion resistance was decreased in contrary to the substrate material	[140]
HAp/MWCNTs	Ti–6Al–4V	The EPD voltage: 5÷30 V; the EPD time: 2÷10 min; the anode "+": substrate; the cathode "−": stainless steel; the content of MWCNTs: 1÷5 wt%; sintered at 800 °C for 2h	Properties: The hardness of the MWCNTs coating containing 1 wt% and 5 wt% of MWCNTs was 6 GPa and 7.12 GPa, respectively, and the Young's modulus of 155 GPa and 160 GPa, respectively. The adhesion strength of the HAp/MWCNTs coating was higher than for the HAp coating	[141]
MWCNTs	Ti13Nb13Zr	The EPD voltage: 20 V; the EPD time: 0.5 min; the anode "+": substrate; the cathode "−": stainless steel; the content of MWCNTs: 0.25 wt%	Properties: The roughness of the coating was 0.34 µm, the hardness of 0.101 ± 0.049 GPa, and Young's modulus of 14.17 ± 4.32 GPa. The coating showed the worst resistance to plastic deformation and accommodation to substrate deflections in comparison with the MWCNTs/TiO_2 and MWCNTs_Cu coatings (described below)	[111]
MWCNTs	Ti13Nb13Zr	The EPD voltage: 11 V; the EPD time: 2 min; the anode "+": substrate; the cathode "−": stainless steel; the content of MWCNTs: 0.27 wt%	Properties: The roughness of the coating was 0.098 µm, the hardness of 0.101 ± 0.049 GPa, and Young's modulus of 14.17 ± 4.32 GPa. The adhesion strength of the coating was assessed using a nano-scratch test and the value of the critical load was 116.5 ± 32.07 mN. The coating was hydrophilic and in the final summary had the best properties in contrast with MWCNTs with additions (described below), when considering an application in endoprosthesis	[142]
MWCNTs	Ti Grade II	The EPD voltage: 20 V; the EPD time: 1 min; the anode "+": substrate; the cathode "−": stainless steel; the content of MWCNTs: 0.25 wt%	Properties: The roughness of the coating was 0.29 µm, the hardness of 0.032 ± 0.0003 GPa, and Young's modulus of 3.41 ± 0.03 GPa. The coating achieved the highest plastic properties in comparison with the base MWCNTs and MWCNTs_Cu coating (described below) and a high ability to accommodate substrate deflections	[143]

Table 5 (continued)

Coating	Substrate	Main parameters	Coating specification	References
MWCNTs–TiO_2	Ti13Nb13Zr	(1) EPD of MWCNTs: the EPD voltage: 20 V; the EPD time: 0.5 min; the anode "+": substrate; the cathode "−": stainless steel; the content of MWCNTs: 0.25 wt% (2) EPD of TiO_2: the EPD voltage: 50 V; the EPD time: 4 min; the anode "+": stainless steel; the cathode "−": a substrate	Properties: The roughness of the coating was 0.65 µm, the hardness of 0.137 ± 0.048 GPa, and Young's modulus of 7.69 ± 1.75 GPa. The coating achieved the lowest ability to accommodate substrate deflections and the lowest resistance to plastic deformation in comparison to the MWCNTs_Cu and MWCNTs/TiO_2 coatings	[111]
MWCNTs/Cu		The EPD voltage: 50 V; the EPD time: 4 min; the anode "+": stainless steel; the cathode "−": a substrate; the content of MWCNTs: 0.25 wt%	Properties: the roughness of the coating was 0.41 µm, the hardness of 0.213 ± 0.061 GPa, and Young's modulus of 10.83 ± 2.12 GPa. The coating achieved the best resistance to plastic deformation in comparison with the base MWCNTs and MWCNTs/TiO_2 coating	
MWCNTs–nanoHAp	Ti13Nb13Zr	(1) EPD of HAp: the EPD voltage: 30 V; the EPD time: 2 min; the anode "+": stainless steel; the cathode "−": a substrate (2) Sintering (3) EPD of MWCNTs: the EPD voltage: 30 V; the EPD time: 2 min; the anode "+": substrate; the cathode "−": stainless steel; the content of MWCNTs: 0.27 wt%	Properties: the roughness of the coating was 0.98 µm, the hardness of 0.022 ± 0.015 GPa, and Young's modulus of 5.63 ± 2.76 GPa. The adhesion strength of the coating was assessed using a nano-scratch test and the value of the critical load was 92.06 ± 34.3 mN. The coating was hydrophobic and in the final summary had worse properties than the base MWCNTs coating when considering an application in endoprosthesis	[142]
MWCNTs–nanoHAp–nanoAg–nanoCu		The EPD voltage: 30 V; the EPD time: 2 min; the anode "+": substrate; the cathode "−": stainless steel; the content of MWCNTs: 0.4 wt%	Properties: The roughness of the coating was 0.618 µm, the hardness of 0.035 ± 0.019 GPa, and Young's modulus of 8.88 ± 3.26 GPa. The adhesion strength of the coating was assessed using a nano-scratch test and the value of the critical load was 60.38 ± 10.21 mN. The coating was hydrophobic and in the final summary had worse properties than the base MWCNTs coating when considering an application in endoprosthesis	
MWCNTs–TiO_2	Ti Grade II	(1) EPD of MWCNTs: the EPD voltage: 20 V; the EPD time: 1 min; the anode "+": substrate; the cathode "−": stainless steel; the content of MWCNTs: 0.25 wt% (2) EPD of TiO_2: the EPD voltage: 50 V; the EPD time: 4 min; the anode "+": stainless steel; the cathode "−": a substrate	Properties: The roughness of the coating was 0.56 µm, the hardness of 0.183 ± 0.0572 GPa, and Young's modulus of 10.11 ± 2.42 GPa. The coating achieved the highest resistance to plastic deformation	[143]
MWCNTs/Cu		The EPD voltage: 50 V; the EPD time: 4 min; the anode "+": stainless steel; the cathode "−": a substrate; the content of MWCNTs: 0.25 wt%	Properties: The roughness of the coating was 0.36 µm, the hardness of 0.079 ± 0.0354 GPa, and Young's modulus of 3.51 ± 1.84 GPa. The coating achieved the highest plastic properties in comparison with the base MWCNTs and MWCNTs_TiO_2 coating and the highest ability to accommodate substrate deflections	
HAp–Si–MWCNTs	NiTi	The EPD voltage: 30 V; the EPD time: 1 min; the anode "+": platinum; the cathode "−": a substrate; the content of MWCNTs: 1 wt%	Properties: The coating showed a uniform and compact structure and the bonding strength was assessed at 27.47 ± 1 MPa	[113]
Mg–14Li–1Al/MWCNTs	Mg14Li1Al	The EPD voltage: 30 V; the EPD time: 5 min; the anode "+": stainless steel; the cathode "−": a substrate; the content of MWCNTs: 0.25 wt%	Properties: The coating properties, such as yield strength, ultimate tensile strength, and elongation were assessed respectively at 213 MPa, 266 MPa, and 21.6%, and were significantly increased in the contrary to the substrate material. The microhardness highest value for the Mg–14Li–1Al/MWCNTs material was 84.6 HV	[144]

Table 5 (continued)

Coating	Substrate	Main parameters	Coating specification	References
Hap–Ti–MWCNTs	NiTi	The EPD voltage: 60 V; the EPD time: 2 min; the electrodes: graphite and substrate; the content of MWCNTs: 1 wt%	Properties: The coating showed improved corrosion resistance and improved fibroblast cell (L929) proliferation in comparison to the NiTi substrate material. The coating demonstrated non-toxicity in the culture medium	[145]
MWCNT/TiO_2–Co	Cooper	The EPD voltage: 80 V; the EPD time: 5 min; the electrodes: platinum and substrate; the content of MWCNTs: 0.02 wt%	Properties: The MWCNT/TiO_2-Co showed a discharge capacity of 305 mAh/g, which is twofold higher than that of pure MWCNTs and 1.6-fold higher than CNT/TiO_2	[114]
MWCNT	Composite pencil graphite	The EPD voltage: 20–25 V; the EPD time: 1–3 min	Properties: The carboxylic MWCNTs has better current density, onset potentials, and charge transfer resistances in contrast to composite pencil graphite electrode and can be used as an electrochemical sensor in the analysis of hyperin	[146]

3.1.4 Low-velocity oxy-fuel thermal spraying

Low-velocity oxy-fuel (LVOF) thermal spraying is very similar to HVOF, except for particle velocities, which are here lower, with close (2300–2500 °C) or the same flame temperatures. At the same time, particle velocities in LVOF are higher than in plasma spraying [91, 101]. Coatings deposited by LVOF are corrosion- and wear-resistant [102].

3.2 Electrochemical methods

The electrochemical methods are among the most simple techniques. The deposition material is a suspension with charged micro- or nanoparticles, which are migrating to the substrate, mainly due to the applied electrical field. Figure 5 demonstrates electrochemical methods, which are mostly used to prepare CNTs coatings and CNTs coatings with additions.

3.2.1 Electrostatic spraying

The electrostatic spraying (electrospray method, ES, shown in Fig. 5C) is a simple technique used to deposit coatings by dispersing charged material under an applied electric field. The deposition system consists of a generator and micro-injector, where a charged coating suspension is placed. Coatings prepared using this method are characterized by good adhesion to the substrate [103].

3.2.2 Electrophoretic deposition

Electrophoretic deposition (EPD) is a simple method carried out in suspension, where two electrodes, an anode, and a cathode are placed parallel to each other and connected usually to a DC power supply (Fig. 5B). Due to the electric field, the particles suspended in the solution migrate to one of the electrodes (depending on particle charge) and coagulate, forming a coating [111, 112, 142, 143, 147].

3.2.3 Electrocathodic deposition

Electrocathodic deposition (ECD), which is also known as electrocathodically-assisted deposition (ECAD), electro-co-deposition, or electrolytic plating is a method used in water solutions of inorganic compounds appearing as cations and anions. Additionally, CNTs (or, e.g., their carboxylated complexes [148]) can be transported by large cationic particles with which they form hydrogen chemical bonds. Under an electric field, the cations or cation–CNTs complexes move toward the cathode being a covered

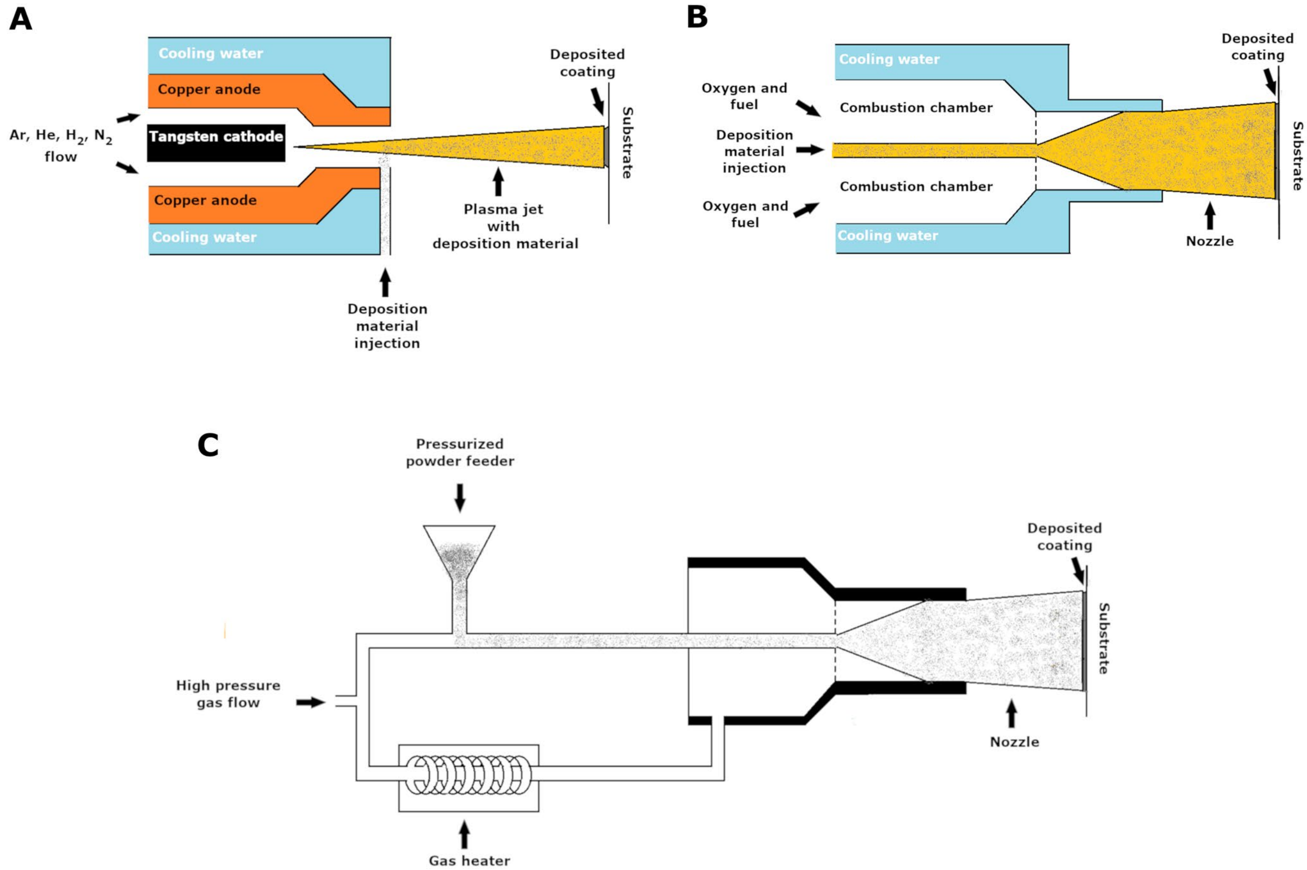

Fig. 4 Schematic illustration of thermal spraying methods: **A** plasma spraying, **B** high-velocity oxy-fuel thermal spraying, and **C** cold spraying

substrate, and form coatings [149, 150]. A schematic diagram of electrocathodic deposition is shown in Fig. 5A.

3.3 Laser methods

High-speed laser cladding (HSLC) is one of the methods applied to prepare CNT coatings, as shown in Fig. 7. Traditional laser cladding (LC) uses laser energy to melt additional material with the surface layer of the substrate. The additional material could be in the form of powder, wire, or strip [104]. LC method allows preparing surfaces free from porosity and cracks [105], but still too thick to produce wear and corrosion protective coatings because the surface preparation rate ranges from 10 to 50 cm^2/min. For ultra-high-speed laser cladding, the rate of cladding is approximately 500 cm^2/min, which is more efficient resulting in coatings of 10–250 µm thick [106]. For better understanding, Fig. 6 schematically demonstrates the idea of the HSLC technique (Fig. 7).

4 Properties of composite coatings

4.1 Topography and morphology

Surface topography is a qualitative feature of a surface shape, which is characterized by a quantitative feature, named surface roughness, expressed by the surface S_a parameter (multiple lines) or line R_a parameter. Table 6 shows a short review of the roughness of CNTs coatings. When discussing topography, it is also essential to point to surface morphology, which describes the coating chemical and phase composition, thus Table 4 also provides such information.

Table 6 shows that the roughness of electrochemically prepared CNTs-containing coatings is lower compared to other methods. Also, the plasma electrolytic oxidation has a lowering effect on the CNT–Al coating image. The microstructure of each coating depends on the method of synthesis. Plasma-sprayed coatings generally have

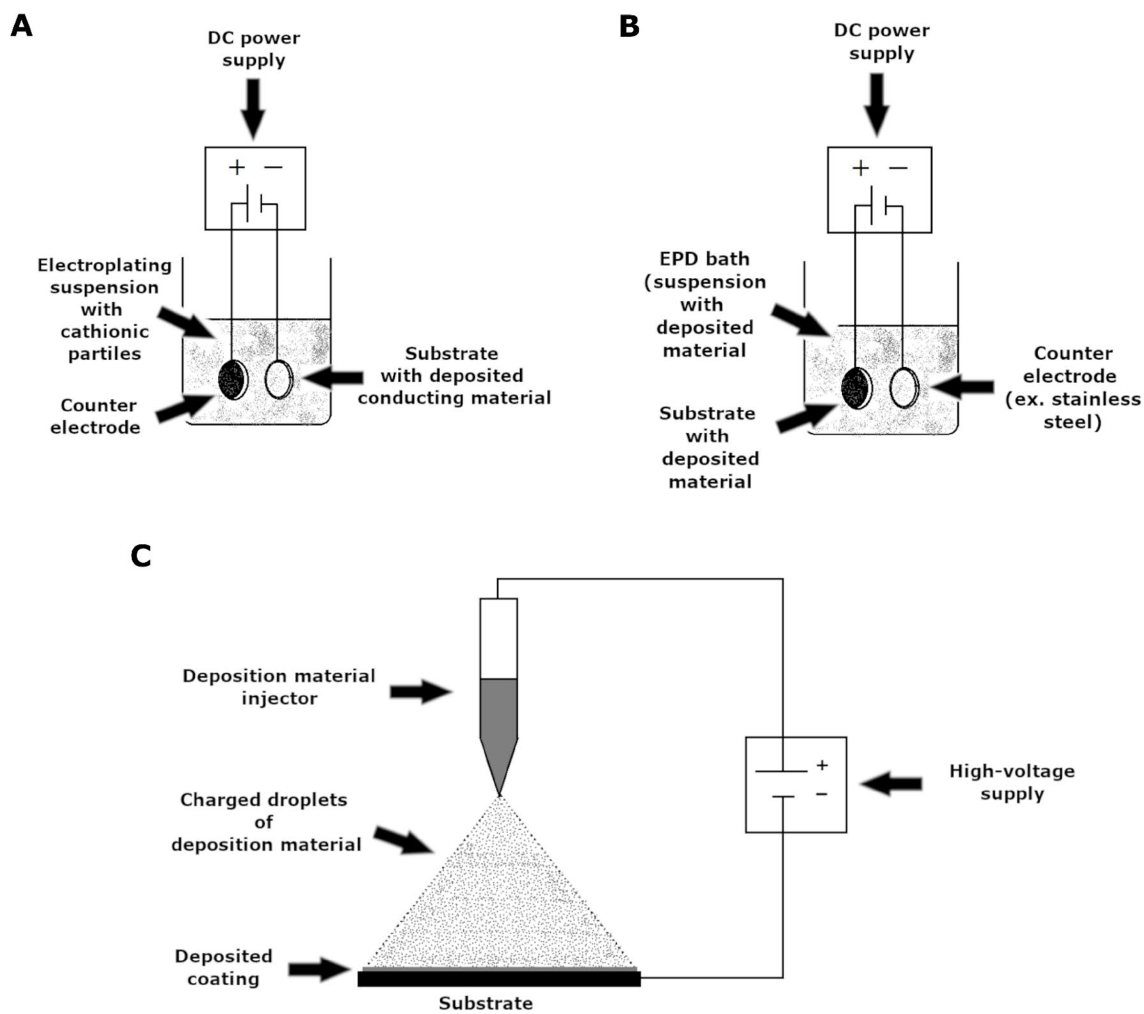

Fig. 5 Schematic illustration of electrochemical methods of CNTs coating deposition: **A** ECD, **B** EPD, and **C** ES

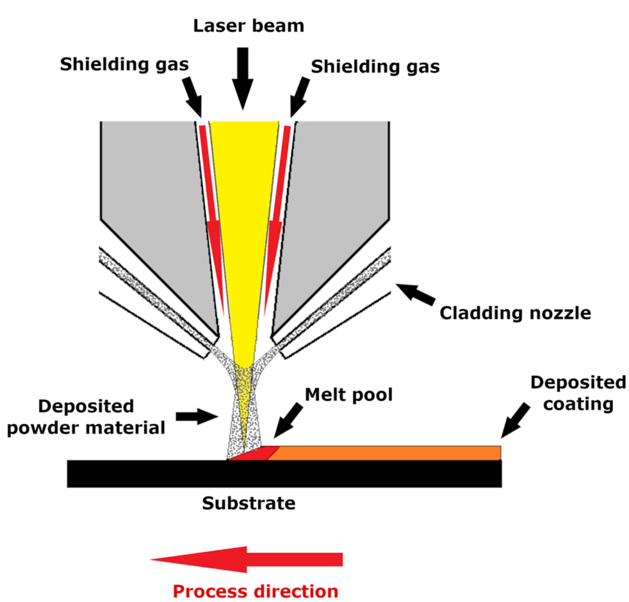

Fig. 6 Schematic illustration of HSLC method of coating synthesis

lamellar microstructure due to layer-by-layer deposition, where some microcracks, voids, and porosity can be distinguished [124, 125, 127, 136]. The porosity of Al–Si–CNTs coatings ranges from 10 to 12% and many agglomerates of size distribution 39÷57 µm could be observed [123]. For Ta_2O_5/CNT coatings the porosity ranges at 18÷26% and increases with the higher concentration of CNTs. Such coatings are intended for biomedical applications and reach a thickness of 540 ± 110 µm [31]. Generally, the coatings prepared using PS show regions, where the powder material is unmelted, partially melted or melted [94, 127]. Another method of CNTs coatings preparation is HSLC which gives coatings almost as flat as the substrate, without cracks in the micro-scale. For nickel-plated CNTs/Fe-based coatings, there could be seen phase transition from the columnar dendrite, through the crystal to amorphous resulting from a temperature gradient, and with the increase of CNTs content, all phases are refined [119]. CNTs coatings prepared with the CS method have

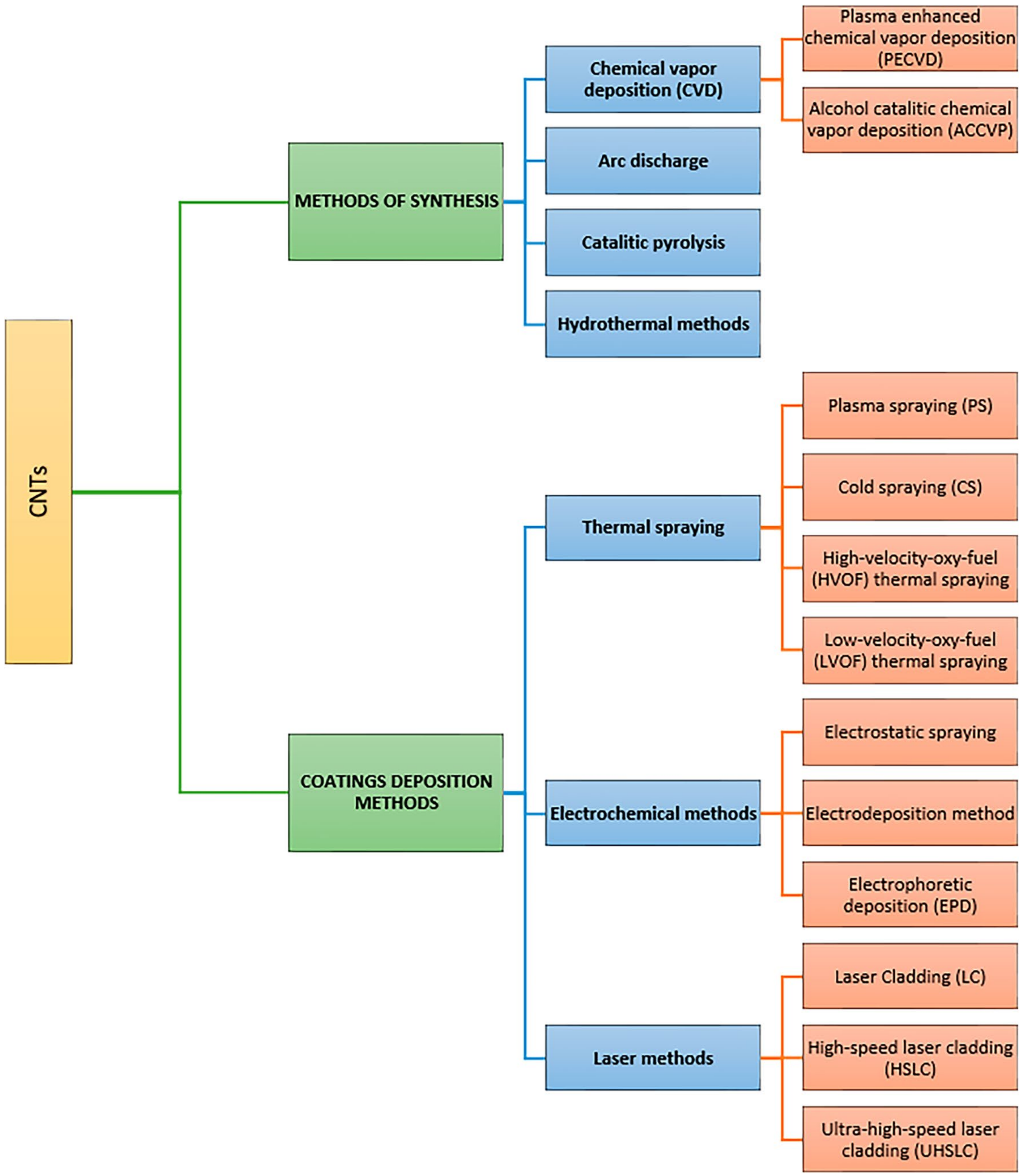

Fig. 7 A scheme of CNTs methods of synthesis and CNTs coatings deposition methods

flake-like morphology, whereas in cross-sectional images lamellar structure could be observed. Xie et al. reported CNT/AlSi coatings thickness to be several micrometers [108]. Moreover, 1wt%-CNT–Al coatings exhibit pores but their number and size are smaller than for the pure Al coating deposited on AZ91 Mg alloy [130]. EPD-prepared coatings have CNTs uniformly distributed. The other components such as nanometals and nanoceramics are mostly agglomerated [111, 142, 143] due to suspension instability and no possibility to stir during the process. Such coatings are also laser-modified, followed by scratches, folds, and bulges observed on their surface. The phases like TiC in the form of dendrites and spheres could be distinguished. The thickness of laser-modified MWCNTs coating was reported to be 7.88 ± 0.35 µm [112].

In materials science, morphology describes the shape, texture, and distribution of different elements and phases at a surface, whereas topography determines the quantitative 3D configuration of different geometrical features on a surface. The studies of both topography and morphology

Table 6 The roughness of coatings with CNTs

Coating	Substrate	Method of synthesis	Ra (μm)	Sa (μm)	Morphology description	References
Cr–CNT[a]	Steel	ECD	0.29	–	A cauliflower-like structure bulged deposit	[136]
Cr–YSZ–CNT[b]			0.22	–	A YSZ and CNTs are well dispersed in the Cr matrix, where a two-phase structure might be observed	
Ta_2O_5/CNT	Ti6Al4V	PS	9.6÷10.5	–	Characteristic to PS method coatings morphology, where layers of Ta_2O_5/CNT splats can be distinguished, homogenous CNTs coating, and uniformly distributed micropores of the distribution ranging from 1 to 5 μm	[31]
Cu–5CNT[c]	Cu	CS	20.69	–	The CNTs are not homogenously dispersed. No cracks observed	[132]
(Cu–5CNT)–10AlN[c]			14.37	–	Both, AlN particles and CNTs are not homogenously dispersed. No cracks observed	
(Cu–5CNT)–20AlN[c]			10.53	–		
CNT–Al	AZ91 Mg	CS + PEO	4.01	–	The structure of the CNT coating is lamellar, with microcracks, and Al_2O_3 volcanic-type pores. There could be distinguished α-Al_2O_3 and γ-Al_2O_3 forms of Al_2O_3 and graphitized carbon. The thickness of the coating is about 25 μm	[107]
MWCNT[d]	Ti13Nb13Zr	EPD	–	0.098	Uniform distribution of CNTs	[142]
MWCNT–HAp[d]			–	0.980	Many agglomerates of HAp observed, stuck to the CNTs	
MWCNT–Hap–nanoAg–nanoCu[d]			–	0.618	Many agglomerates of nanometals adsorbed to HAp particles	
MWCNTs[d]			–	0.34	Uniform distribution of CNTs. The thickness of the coating is about 0.5 μm	[111]
MWCNTs–TiO_2[d]			–	0.65	Uniform distribution of CNTs, many agglomerates of TiO_2 of micron size. The thickness of the coating is about 2 μm	
MWCNTs–Cu[d]			–	0.41	Uniform distribution of CNTs, the Cu nanoparticles located at the crossover of MWCNTs causing cracks. The thickness of the coating is not uniform; there are places of narrower and thicker coating	
MWCNTs[d]	Ti Grade II	EPD	–	0.353	Uniform distribution of CNTs	[143]
MWCNTs–TiO_2[d]			–	1.033	Uniform distribution of CNTs, many agglomerates of TiO_2 of micron size	
MWCNTs–Cu[d]			–	0.495	Uniform distribution of CNTs with Cu agglomerates built into	

[a]The roughness of the Cr surface is about 0.90 μm

[b]The roughness for Cr–YSZ is about 0.86 μm

[c]The roughness of the Cu surface is about 17.5 μm

[d]The roughness Sa parameter of Ti13Nb13Zr surface is about 0.203 μm

are always immanent parts of any materials investigations as their influence on bioactivity, i.e., bone growth rate, and also on corrosion behavior, is crucial. It might be assumed that in topography, the deciding is the proper development of the surface. For titanium, the geometry and dimensions of oxide nanotubes are important. In particular, the walls of rough and sharp nanotubes TiO_2 provide suitable places for the nucleation of biospecies [151]. The presence of titanium dioxide in the form of nanopatterns with heights of about 1.5 nm and nanotubes influenced protein adsorption kinetics and the thickness and morphology of the resulting protein layer which was attributed mainly to electrostatic interactions [152, 153]. The nanopatterned arrays developed by the chemical hydrothermal process at high temperatures mimic the dragonfly wing and are suggested as the origin of their activity against different bacteria [154]. The shot peening of titanium causes the substantial appearance of the micro- and nanoscale oxide layers which strongly affect adhesion, proliferation, and osteogenic differentiation of human cells, additionally enhancing wettability [154]. But not only the presence of titanium oxide is a necessary condition for positive effects of topography. Osteoblasts showed a tendency to accelerate their proliferation on titanium spike structures [155]. The positive effects of the surface morphology, and micro and nano roughness, which improved osseointegration, were observed for hard titanium [155]. The additive designed manufacturing such as powder bed fusion (PBF) metal 3D printing makes porous structures of different local surface topography and pore shape that affects cell proliferation and differentiation. In particular, titanium with pores triangular and rectangular pores has higher roughness with a structure more concave (valley-like) than that with circular pores and effectively promotes the proliferation and differentiation of osteoblasts, thus improving osseointegration strength and implant fixation [156]. Similar phenomena were observed for porous topography for silicon [157, 158], hydroxyapatite [159, 160], poly(L-lactide) (PLLA) modified with femtosecond laser [161], poly(methyl methacrylate) (PMMA) [162]. For CNTs layers or composite coatings, there have been no important investigations, but it might be assumed that the presence of CNTs can enhance biological processes.

4.2 Adhesion between CNTs and metallic substrate

4.2.1 Adhesion mechanisms

The adhesion strength is mainly determined by mechanical and thermal interaction between particle and substrate depending on the method of coating synthesis. In the CS method deposition velocity and, thus, the degree of deformation plays an important role. At the critical velocity, the material is plastically deformed and a region (called adiabatic shear instability) where the temperature could reach the melting point of the material is formed, leading to viscoelastic material flow, formation of a conformal interface, and metallurgical bonding. Thus, the evaluation of adhesion strength is dependent on the particle velocity, particle or substrate temperature, substrate roughness, particle morphology, and mechanical properties of both the particle and the substrate [95, 163].

The CNTs formulate a mesh structure, with a large surface area, giving space for reaction. Direct reaction of CNTs with plasma plume in plasma spray method resulted in the generation of defects which leads to an increase in reaction sites [123]. In this method, there are seen three typical microstructures: fully melted region, partially melted region, and pores. In the fully melted region, some reduction processes may occur such as in the case of CNT–TiO_2 coating for which the carbothermal reduction appears followed by the formulation of some $TiO_{2\text{-}x}$ species. In partially melted regions, CNTs and the other components stick to each other and bond with weak van der Waals forces [94].

Adhesion plays a very important role in implant coating. If the adhesion is poor, during implantation surgery the coating can be degraded or even totally removed. Therefore, even further properties are positive, the adhesion must be sufficient enough to counteract mechanical stresses during the insertion of whatever implant into the bone. Below different methods are described which are used to assess the anticipated integrity by measurements of the adhesion strength of the coating to the bone. Besides, as the coating is subject during surgery and after different loads, the coating must be also tough, but not brittle. Therefore, CNTs are added mainly to improve rigidity, hardness, and toughness.

Despite several described below tests to calculate adhesion strength, widely described in the literature, however, the best assessment of the coating behavior during implantation surgery is in vivo experiments on animals. The results of such successful studies are, however, not frequent. It is noted that to increase the clinical success rate of metal implants is to increase their bone-bonding properties, i.e., to develop a bone bioactive surface leading to reduced risks of interfacial problems. Much research has been devoted to modifying the surface of metals to make them bioactive. Many of the proposed methods include depositing a coating on the implant. However, there is a risk of coating failure due to low substrate adhesion. In [164], a method to obtain bioactivity combined with a high coating adhesion via a gradient structure of the coating [165]. The review of different techniques for HAp coatings on Ti6Al4V alloy, mostly still applied for hip joint implants, showed that three techniques, namely sputtering, IBAD (ion beam-assisted deposition) followed by heat treatment, and EPD give reasonably high adhesion values. To increase the adhesion, the substrate is usually properly prepared to develop its surface area and create micro and nanoforms such as grooves, pillars, columns, etc., by mechanical grinding, acidic and alkaline etching, chemical, electrochemical, and micro-arc oxidation, laser roughening, and patterning. In [166], such laser micromachining of titanium and its alloys created micro-grooves of diameter of about 10 µm, and then coating with arginine–glycine–aspartic acid to enhance cellular spreading and adhesion was deposited. The laser-grooved and coated rods had significantly higher pull-out strength than the only laser-grooved and control rods. This paper in an excellent way explains the core of this problem. To summarize, the coating for long-term implants must demonstrate several features, such as the bioactivity necessary to form quickly and strongly the bond between an implant and bone, mechanical behavior against anticipated stresses sufficient to avoid any serious damage or degradation, and high adhesion. Truly, we would like to achieve only bioactivity without cytotoxicity, but weak mechanical strength or weak coating adhesion might cause the coating to be destroyed and the main aim for its deposition will vanish.

4.2.2 Testing methods and adhesion strength of CNTs

Among different methods used to assess the adhesion of coatings, the standard ASTM F1044 based on shear testing of calcium phosphate and metallic coatings is the most often applied for CNTs composite coatings. It assesses the adhesion of coatings to substrates or the cohesion of a coating under shear stress to the interface. Commonly flat-coated specimens are glued to a proper counterpart and loaded up to the division of both parts. The more recent results of such investigations are shown in Table 7. The addition of the CNTs results in a significant increase in the adhesion strength, but as a rule at its higher contents or if a third component is present in a coating.

Exceptionally, the standard test method based on measuring adhesion force by tape test, ASTM D 3359-08, was applied for the chitosan–nanoHAp–CNTs on Ti substrate [171]. The tape tests displayed high adhesion strength (class 5B).

Nanoscratch testing is increasingly applied [141, 142] despite that mechanical force and not stress is measured which makes the results not comparable to those based on the shear technique. For the nanoHAp–CNTs coatings deposited on Ti and its alloys, [141], a critical load of 350 mN was noticed for the HAp–5% CNTs coating. In the other research [142] the values of critical force resulting in the delamination of coatings deposited on Ti13Nb13Zr alloy were 116.5 mN, 90.2 mN, and 60.4 mN under shear stress for CNTs, CNTs–HAp, and CNTs–nanometal coatings, respectively, at 0.27 wt% of CNTs only.

Finally, it is to emphasize a novel technique, called a nanomechanical pull-out method [172] that has used an atomic force microscopy cantilever acting as a force sensor and mounted vertically to a 3D piezo nanomanipulator. The interfacial shear strength and the maximum load-bearing capacity of the CNTs coatings on Al Ti and Zn substrates were 217 and 245 nN, and after quantitative analysis of the results, the shear stresses at the interfaces were calculated as 31÷40.01 MPa, depending on heat treatment, and 37.8 MPa, respectively [172, 173]. Based on the ASTM C-633 standard (European EN 582) and using the tensile tester for pull-out samples, the adhesion between cold-sprayed CNTs to Al matrix was assessed at 15–18 MPa [95].

Systematic research on the effects of some features and amounts of CNTs composites is rare. One of the reasons for increasing the adhesion strength with increasing the CNTs content in HAp coating is bridging formed by CNTs between coating and substrate [174, 175]. It is noted that an addition of CNTs has also been proposed for protective coatings based on epoxy resins [16].

Table 7 The shear strength of CNTs-containing coatings, determined by ASTM F1044 standard

Coating composition	Substrate	Shear strength (MPa)	References
HAp–20 wt% MWCNTs	Ti	34.94	[167]
HAp–30 wt% MWCNTs	Ti	35.44	[167]
HAp	Ti	20.62	[167]
HAp–0.1MWCNTs	Ti	19.0	[168]
HAp–1MWCNTs	Ti	24.2	[168]
HAp–2MWCNTs	Ti	22.4	[168]
HAp	Ti	18.1	[168]
HAp–0.1SWCNTs	Ti	17	[169]
HAp–0.3SWCNTs	Ti	~21	[169]
HAp–0.5SWCNTs	Ti	25.7	[169]
HAp-1.0SWCNTs	Ti	~25	[169]
HAp	Ti	15.3	[169]
HAp–20Si–1MWCNTs	NiTi	27.5	[113]
HAp–1MWCNTs	NiTi	19.3	[113]
HAp–20Si	NiTi	23.2	[113]
HAp	NiTi	18.0	[113]
HAp–20Ti–1MWCNTs	NiTi	32.1	[170]
HAp–20Ti	NiTi	~27	[170]
HAp	NiTi	17.2	[170]
HAp–Ta_2O_5–0.5MWCNTs	NiTi	30.2	[57]
HAp–Ta_2O_5–1MWCNTs	NiTi	32.4	[57]
HAp–2Ta_2O_5–1.5MWCNTs	NiTi	32.7	[57]
HAp–Ta_2O_5–2MWCNTs	NiTi	34.6	[57]
HAp–Ta_2O_5	NiTi	23.7	[57]
HAp	NiTi	18.9	[57]

4.3 Mechanical behavior

The mechanical behavior of a material is one of the most important features discussed when the material is considered for use in biomedical applications. Microhardness, nanohardness, elastic (Young`s) modulus, and yield strength less often, are the mechanical properties checked to describe the material and attribute it to an application. The difference between micro- and nanohardness is the area of the test. Microhardness gives information about the average hardness of a large area, while nanohardness is more specific and describes the little area using smaller loads. Young's modulus is used to assess material stiffness and is a very important factor in terms of biomedicine because the mismatch of implant and bone in Young's modulus could lead to complications for the patient and even the necessity to repeat the surgery. Usually, scientists are looking for materials, with lower values of elastic modulus than the natural bone elastic modulus, which is for cancellous bone about 3.78 GPa and cortical bone about 14.64 GPa [176]. Table 8 shows the mechanical properties of coatings composed of CNTs.

Table 8 Research of CNT-composite coatings deposited on a metallic substrate

Coating	CNTs wt%	Substrate	Microhardness (GPa)	Nanohardness (GPa)	Elastic modulus (GPa)	Yield strength (GPa)	References
Al–5CNT	6.2	Mild steel	1.350 ± 0.05	2.33 ± 0.27	107 ± 6	38.3 ± 1.9	[123]
Al–10CNT	12.4	Mild steel	2.100 ± 0.04	2.89 ± 0.27	125 ± 7	41.5 ± 1.8	
Al–Si–5CNT	5.0	Mild steel	–	–	107 ± 6	8.3 ± 1.9	[124]
Al–Si–10CNT	10.0	Mild steel	–	–	125 ± 7	41.5 ± 1.8	
CNT–Al	1.0	AZ91 Mg alloy	–	1.66 ± 0.2	77.6 ± 3.3	–	[130]
CNT–Al[a]	1.0	AZ91 Mg alloy	13.9	–	185.4	–	[107]
Cr–CNT	2	Steel[b]	15.0 ± 1.2	19.0÷3.0	196.0 ± 8.2	–	[137]
Cr–YSZ–CNT	2	Steel[b]	25.0 ± 0.28	32.0 ± 3.4	206 ± 11	–	
Cr–CNT	2	Steel[b]	14.0÷1.7	–	192÷22	–	[136]
Cr–YSZ–CNT	2	Steel[b]	24.0÷1.5	–	210÷20	–	
CNTs	0.5	Ti[c]	1.664 ± 0.107	–	101 ± 15	–	[140]
MWCNT	0.27	Ti13Nb13Zr[d]	–	0.101 ± 0.049	14.17 ± 4.32	–	[142]
MWCNT–HAp	0.27		–	0.022 ± 0.015	5.63 ± 2.76	–	
MWCNT–HAp–nanoAg–nanoCu	0.4		–	0.035 ± 0.019	8.88 ± 3.26	–	
MWCNT	0.25		–	0.101 ± 0.049	14.17 ± 4.32	–	[111]
MWCNT–TiO_2			–	0.137 ± 0.048	7.69 ± 1.75	–	
MWCNT–Cu			–	0.213 ± 0.061	10.83 ± 2.12	–	
MWCNT	0.25	Ti Grade II	–	0.032 ± 0.0003	3.14 ± 0.03	–	[143]
MWCNT–TiO_2			–	0.183 ± 0.0572	10.11 ± 2.42	–	
MWCNT–Cu			–	0.079 ± 0.0354	3.51 ± 1.84	–	

[a]The coating was first prepared by CS and second by PEO

[b]The elastic modulus for stainless steel is about 51.07 GPa [176]

[c]The elastic modulus for Ti is about 50.20 GPa [176]

[d]The elastic modulus for Ti13Nb13Zr is of 83.32 ± 11.63 GPa

CNT-based coatings are deposited on different substrates with variable CNTs and other additions` contents. Considering the value of Young's modulus of CNT-containing coatings for application in biomedicine we can observe that the coatings with 0.25 and 0.27 wt% addition of CNTs revealed elastic modulus values similar to cortical bone. The addition of nanometals and nanoceramics causes a decrease in Young's modulus. The CNTs applied in the YSZ and Al-based coatings improve mechanical properties [125, 130]. For Al-based coatings, the CNTs enhance coatings properties through thermal expansion mismatch, and Orowan looping as CNTs are generating high dislocation density and limit dislocation migration. Also, CNTs play a reinforcing role, dependent on content and distribution [130].

4.4 Corrosion resistance

The corrosion resistance testing focuses on the electrochemical behavior of the deposit by, almost exclusively, the electrochemical potentiodynamic polarization test. The increase in current density means the corrosion resistance decreases. The conditions of the test can be changed, such as temperature, electrolyte composition, scanning rate, and potential range. For biomedical applications mostly the temperature of the body is imitated and SBF solution is used as an electrolyte. Before the main test, the open circuit potential (OCP) value is checked, which is the potential at zero current value and gives information about the thermodynamic stability of the examined material. Mostly OCP value is negative, but sometimes it could be positive, which means a passivation phenomenon of the coating can occur [136]. The OCP value also gives a clue about the potential range that should be used during the electrochemical polarization test. Table 9 shows a brief conclusion about the corrosion behavior of CNTs-based coatings.

For the coatings with YSZ, Cr, and Al prepared using PS the addition of CNTs enhanced the corrosion resistance [125, 127, 130, 136]. Tripathi et al. [136] reported better corrosion resistance for the Cr–CNT and Cr–YSZ–CNT compared to the bare Cr material, with the highest potential achieved for the Cr–YSZ–CNT coating. For the Cr substrate the corrosion current density and corrosion potential

Table 9 A state-of-the-art corrosion behavior of CNT-containing coatings

Coating	Substrate	Crucial parameters of coating preparation	E_{corr} (V)	I_{corr} (nA/cm^2)	References
CNTs–TiO_2	Ti13Nb13Zr	EPD (0.25% CNTs, TiO_2 0.15 g, 50 V, 4 min)	−0.169	1.4	[177]
		EPD (0.25% CNTs, TiO_2 0.15 g, 60 V, 4 min)	−0.282	206.4	
		EPD (0.25% CNTs, TiO_2 0.30 g, 50 V, 4 min)	−0.217	17.5	
		EPD (0.25% CNTs, TiO_2 0.30 g, 60 V, 4 min)	−0.439	9.85	
CNTs		EPD (0.25% CNTs, 20V, 30 s)	−0.233	176.2	
NiTi + HAp–Ti–CNT	NiTi	EPD (1% CNTs, 60 V, 2 min)	−0.0391	0.91	[145]
Cr–CNT	Cr	ECD (20 g/L of CNTs)	−0.509	6900	[136]
Cr–YSZ–CNT	Cr	ECD (25 g/L of 3 mol% Y_2O_3, 20 g/L of CNTs)	−0.470	7200	
CNT–Al	AZ91 Mg alloy	CS (1 wt% CNTs)	−0.941	2030	[130]
CNT–Al	AZ91 Mg alloy	CS + PEO (1 wt% CNTs)	−1.126	3734	[107]
CNT	Ti	EPD (28V, 30 s)	0.270	112	[140]
Nickel-plated CNTs/FeCoNbBSi	45 steel	HSLC (0.25 wt% CNTs)	−0.592	547	[119]
Nickel-plated CNTs/FeCoNbBSi	45 steel	HSLC (0.5 wt% CNTs)	−0.502	454	
Nickel-plated CNTs/FeCoNbBSi	45 steel	HSLC (1 wt% CNTs)	−0.518	436	

were 15.9 ± 3.7 μA/cm^2 and − 534 ± 19 mV, respectively, and for Cr–CNT 6.9 ± 1.3 μA/cm^2 and − 509 ± 23 mV, and Cr–YSZ–CNT 7.2 ± 0.9 μA/cm^2 and − 470 ± 13 mV, what gives information that two-phase boundaries inhibit the cracks and limits corrosion [136]. On the other hand, the increase of MWCNTs content in MWCNTs/PU coatings increases the corrosion current density, thus weakening the corrosion resistance. This phenomenon could be explained by the formulation of micro-defects in the PU matrix, which facilitate the substrate metal corrosion. The maximum corrosion rate for MWCNTs/PU coating deposited on Q235 steel is at 8 wt% of MWNCTs and the maximum corrosion resistance appears for 2 wt% of MWCNTs [110]. The same effect was seen for 1 wt%-CNT–Al coating deposited on AZ91 Mg alloy, achieved using the CS method according to the substrate and pure Al coating. The phenomenon was explained by thermal mismatch between the Al matrix and CNTs, which can strengthen the matrix, limit dislocation looping, and suppress crack propagation [107, 130]. Maleki-Ghaleh et al. [145] prepared HAp–Ti–1wt%-MWCNTs coating using the EPD process on NiTi substrate, which possessed the best corrosion resistance in comparison to the substrate and coatings without MWCNTs addition. Nevertheless, there are the same reports about CNT coating EPD-deposited on Ti, which decreases corrosion resistance, due to the porous fibrous structure of the coating and the presence of TiO_2 [140]. Thus, the results are ambiguous indicating the complex roles of components and microstructure, roughness, and uniformity of the surface.

Another method to check corrosion resistance on a micro-scale is the scanning Kelvin probe. The test allows for achieving information about electron work. The higher the escape electron work is, the higher the corrosion resistance. The test indicated the best corrosion resistance for the CNTs/Fe-based coating with 1 wt% of CNTs prepared by HSLC, confirmed by the electrochemical corrosion test. The increase in CNT content caused the decrease in corrosion current density, and the CNTs presence allowed to join the cracks improving corrosion resistance [119].

4.5 Wettability

The contact angle is used to describe the wettability of CNTs coatings. The higher the contact angle is the higher the wettability of a surface, and thus such a surface is named hydrophilic. In the literature, the contact angle between 40 and 60° is the best in terms of promoting cells adhesion and improving the bioactivity of the coating [178]. Lin et al. reported on the decrease in contact angle of the Ta_2O_5/CNT coating deposited on Ti6Al4V to 1÷3° [31]. The wettability of Cu–CNT–TiO_2 coating is also hydrophilic (the contact angle value is 12.85°), due to the presence of TiO_2 particles [135]. The pure CNT coatings prepared using the EPD technique deposited on Ti13Nb13Zr are also hydrophilic and their contact angle is about 56°, while the contact angle of CNTs coatings with HAp and nanometal additions highly increases to hydrophobic values, which is unwelcome in biomedical applications [142]. The impact of laser modification on the wettability of CNTs coatings was also checked and revealed the increasing contact angle to the value of about 80° [112]. The wettability of CNTs coatings is then strongly dependent on the bonding effect and the method of synthesis. Most MWCNTs used to prepare coatings employing electrochemical methods are functionalized to give a negative charge and enable the deposition. Such a modification and changes in the pH of the solution during the process may impact the linking of CNTs to other components of the suspension, thus changing the contact angle of the coating

[142]. On the other hand, the wettability of CNTs coatings is dependent on the roughness.

4.6 Bioactivity and cytotoxicity

Most commonly the MWCNTs' bioactivity and cytotoxicity, namely positive and negative effects on adhesion, viability, proliferation, and mortality of cells were tested in human umbilical vein endothelial cells (HUVECs). Zhao et al. [52] examined three types of MWCNTs with different diameters, named XFM4 (diameter: 10–20 nm), XFM22 (length: 0.5–2 µm; diameter: 20–30 nm), and XFM34 (length: 0.5–2 µm; diameter: > 50 nm) and concluded that the smallest diameter, the higher level of cytotoxicity, the HUVECs are the most internalized, the level of cytokine released is the highest. They also observed the highest level of ER stress biomarkers, due to the highest specific surface area of the MWCNTs, causing autophagy of HUVECs, thus eliminating MWCNTs with such dimensions to be applied in biomedicine, especially in blood vessels. Also, the dose-dependence impact on cytotoxicity was seen. The MWCNTs with the smallest diameter exposed cytotoxicity at concentrations higher than 16 µg/mL. On the other hand, for higher MWCNTs diameters, a greater content of MWCNTs caused higher cytotoxicity to HUVECs, while its addition didn`t indicate obvious changes in the ultrastructure of HUVECs cells.

The MWCNTs diameter cytotoxicity impact on the other cells was also checked for NR8383 cells (normal rat alveolar macrophage cells) [179] and human mesothelial cell lines (MeT5A, E6/E7, and hTERT-immortalized human peritoneal mesothelial cells) [180] and the length impact of MWCNTs on cytotoxicity to HUVECs was investigated. Long et al. [181] examined two types of MWCNTs (XFM19 of length 10–30 µm and XFM22 of length 0.5–2 µm, both outer diameter of 20–30 nm and inner diameter of 5–10 nm) with different concentrations from 2 to 32 µg/mL. The longer the MWCNTs were, the higher level of cytotoxicity to HUVECs, the higher oxidative stress, the higher level of THP-1 monocyte adhesion to MWCNTs, the higher level of ER stress biomarkers were observed, which gives information about the inflammation-inducing effect of longer MWCNTs species. Another parameter discussed in the literature is a surface modification of MWCNTs, which could affect interaction with proteins and cells [182]. According to Sun et al. [183], pristine MWCNTs (XFM19, diameter: 28.97 nm, average length: 1181.14 nm), hydroxylated MWCNTs (XFM20, diameter: 30.46 nm, average length: 1323.94 nm), and carboxylated MWNCTs (XFM21, diameter: 31.03 nm, average length: 1256.59 nm) are cytotoxic to HUVECs and induce oxidative stress to a similar extent while used with MWCNTs concentration of 32 µg/mL or 64 µg/mL. Dinc et al. reported the functionalized (oxidized) MWCNTs were less toxic to HUVECs and MDA-MB-231 cells (breast cancer cells) than pristine MWCNTs [182]. Thus, MWCNTs with a longer length and smaller diameters could induce cytotoxicity to HUVECs, regardless of the type of used functionalization of MWCNTs. However, Dlugon et al. [140] checked the biological activity of CNTs coatings EPD deposited on Ti using the human osteoblast NHOst cell line and after 7 days observed higher cell viability for CNTs modified Ti than for pure substrate. Also, the SWCNTs were investigated in terms of cytotoxicity and showed that the oxidized SWCNTs caused malformed placentas in female mince already after administration of 100 ng/ml of oxidized SWCNTs [184, 185].

The toxicity of MWCNTs is then dependent on their dimensions, such as the diameter, length, and also physicochemical properties, like surface chemistry, and dose. So far studies show that the examined parameters in terms of cytotoxicity are: (1) the internalization of MWCNTs to human cells, (2) the release of inflammatory cytokines (THP-1 monocyte), (3) the mechanism of cytotoxicity activation-reactive oxygen species (ROS) or activation of endoplasmic reticulum (ER) stress biomarkers, such as *ddit3* (DNA damage-inducible transcript 3) or other named *chop* (C/EBP homologous protein); *xbp-1s* (spliced X-box binding protein 1), and the protein level of BiP (binding immunoglobulin protein; GRP78, 78 kDa glucose-regulated protein) [52, 181, 183].

The cytotoxicity is a serious problem that has been attempted to limit by several solutions. In [186] the toxicity of CNTs was shown to be mainly related to their dimensions: toxicity decreases with increasing length of the nanotubes. The toxicity was also reduced for CNTs of small diameter [187], thus the use of smooth CNTs is favorable. Besides this passive way, the functionalization of CNTs is likely the single approach to decrease cytotoxicity, with effectiveness dependent on chemical structure. The carboxylic SWCNTs and MWCNTs, with cytotoxicity investigated by adsorption of human serum albumin [188], of bovine serum albumin [189, 190], and by MTT assay [191] were the least toxic as compared to hydroxylated SWCNTs and amined SWCNTs. The natural bio-resin shellac applied for the functionalization of CNTs also reduces cytotoxicity [192].

The bioactivity of CNTs has been seldom investigated as elementary carbon is an inert body. The high surface properties, including the creation of chemical covalent or van der Waals bonds, are achieved due to nanosized tubes. However, it is now well known that to make CNTs bioactive, chemical functionalization is necessary. There are several indirect evidence for an enhancement or improvement of bioactivity by CNTs in multicomponent coatings. In [193] the multivalent polyanion-dispersed CNTs were used after their functionalization with polyglycerol sulfate and deposited on PCL. That results in higher neural differentiation efficiency creating then highly bioactive nanostructured fibrous scaffolds. In [194] low-dimensional nanomaterials such as CNTs or graphene exhibited noticed in vitro bioactivity and osteoinductivity. In [195] polymer–bioglass–CNTs composite material was investigated. The results showed that the presence of MWCNTs in low quantities enhanced osteoblast-like cell attachment and proliferation compared to composites with high concentrations of MWCNTs, and the mechanism of CNTs-enhanced bioactivity is unclear. Considering the test results for [196] the coatings composed of functionalized multi-walled carbon nanotubes (f-MWCNTs) and hydroxyapatite on 316L steel, it was concluded that the addition of f-MWCNTs in the HAp increases the number of active sites responsible for the formation of carbonated apatite layer. In [197], the use of functionalized carbon nanotubes in the hybrid composition of chitosan/silica showed favorable tissue responses of the CNT-incorporated membrane.

The bioactivity is most often checked using in vitro tests, mostly in SBF solution. Lin et al. [31] reported a complete coverage by hemispherical-shaped particle samples of Ti6Al4V coated with Ta_2O_5 and Ta_2O_5/CNTs. Nevertheless, there could be an observed relationship between the increasing content of CNTs in the coating and with decreasing size of adhered apatite particles. The same team checked the adhesion of osteoblast-like cells, such as osteosarcoma MG-63 cells, which showed satisfactory adhesion and spreading behavior after 7 days of culture, but without an impact of CNTs presence. It means that CNT-decorated coatings could promote cell proliferation and differentiation, and thus they are candidates for use in biomaterials [183].

4.7 Antibacterial efficiency

CNTs have been reported to exhibit killing properties over a wide range of bacteria including human pathogens such as *Escherichia coli* (*E. coli*), *Salmonella typhimurium*, *Bacillus subtilis* (*B. subtilis*), *Staphylococcus aureus* (*S. aureus*), *Micrococcus lysodeikticus* and *Streptococcus mutans*. Several studies have disclosed that pristine CNTs exhibit antibacterial activity by physical contact and collisions leading to puncturing of the bacterial cell membrane and its damage [198, 199]. It was reported in [198] that the force of 100 nN is enough to make AFM-detectable holes in bacteria cells, even though the checked force is unrealistic to appear between bacteria and CNTs in normal conditions, thus this mechanism is unlike. The second mechanism assumed the CNTs are connecting to the bacteria cell membrane in the form of CNT dense network, thus changing cell membrane architecture, and its mechanical properties [198–200]. Liu et al. reported the SWCNTs after 10 min of exposure to *E.coli* and *B. subtilis* increasing cell wall roughness, causing increased cytoplasm leakage and bacteria cell death after 120 min [198], while Schifrano et al. reported a significant reduction of cell number after 24 h incubation in contact with CNTs [200]. Further investigation leads to the assertion that the antibacterial activity of CNTs is light-dependent [201, 202]. Rajavel et al. reported that the SWCNTs and MWCNTs are ROS generators (producing singlet oxygen $^1O_2$, superoxide anions $\dot{O}^{2-}$ and hydroxyl radicals $\dot{O}H$) in sunlight with a light intensity of 903 lm/m^2 and ambient light of 180 lm/m^2 [201]. Such ROS production increases oxidative stress, makes bacteria cell membrane disruption (due to lipid peroxidation) and causes bacteria death [200–202]. Nevertheless, the antibacterial effectiveness of CNTs also depends on bacteria peptidoglycan cell wall thickness and strain resistance, showing the CNTs antibacterial properties are more significant for Gram-negative bacteria (e.g., *E.coli*, *P. aeruginosa*) than Gram-positive ones (e.g., *S. aureus, B. subtilis)* [198, 200]. The above mechanisms of antibacterial activity of CNTs are well established in [200], where both the mechanical injury and ROS production play important roles in the bactericidal effect of CNTs. Figure 8A shows a diagram, summarizing the antibacterial mechanisms of CNTs.

There are many reports about the antibacterial efficiency of CNTs with additions, where the main mechanism of antibacterial efficiency is again the generation of ROS. The cellulose acetate (CA)-CNT–Ag [203] was shown as effective against *E. coli* and *S. aureus*, with the CA matrix creating protection against the harmful effects of silver (i.e., argyria and argyrosis) [203]. Also, CNTs–Ag composites exhibit antibacterial properties against *E.coli* [204]. The addition of CNTs to Ag colloid lowers the minimal inhibitory concentration value of Ag particles in suspension, both against Gram-negative and Gram-positive bacteria. Here, a good dispersion of the Ag nanoparticles on the CNTs is the reason for the high antibacterial activity of CNT–Ag composites [204]. There is evidence about the antibacterial activity of MWCNTs–Ag composites against *E. coli* [205–207], *S. aureus* [203, 208–211], *Staphylococcus haemolyticus* [212], and also against *B. subtilis* and *Pseudomonas aeruginosa* [213]. The other CNTs-containing coating components were reported to have antibacterial properties [212], in particular for composite coatings such as the CNTs–ZnO [214, 215], hydroxyapatite/ZnO/CNT [216], Co doped-ZnO/MWCNTs [214] and MWCNTs–Ag/TiO_2 [217] against *E. coli* and *S. aureus*. Also, the MWCNTs–TiO_2 [218] and Ag–TiO_2–MWCNT [219] were lethal to *E. coli*, and CNTs/TiO_2/polyurethane films to *S. aureus* [220]. Also, SWCNTs composites with Ag nanoparticles inhibited the growth and multiplication of bacteria, such as *S. aureus*, *B. cereus*, *E. coli*, and *P. aeruginosa* [221]. Zhu et al. reported very strong antibacterial performance of SWCNTs in combination with silica and Ag against *E. coli* and *S. aureus* [222]. The same antibacterial activity showed SWCNTs–Ag/TiO_2 hybrids [217]. Although CNT

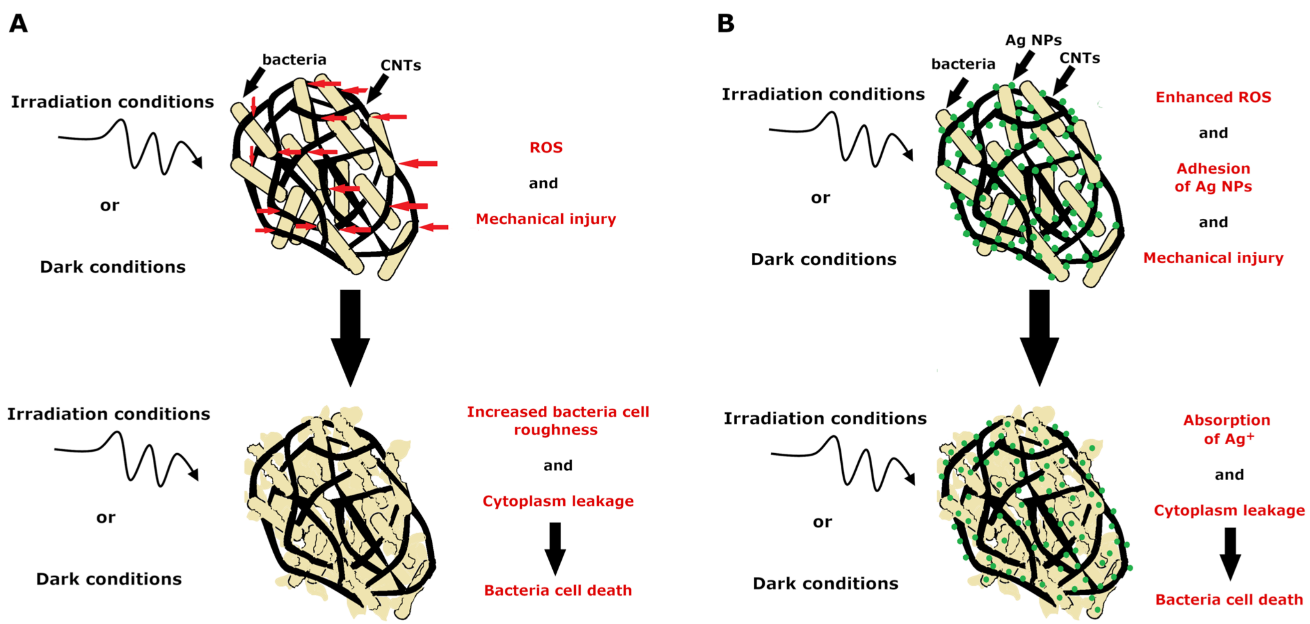

Fig. 8 A schematic illustration of antibacterial mechanisms for **A** CNTs and **B** CNTs with Ag NPs addition

coating improves cell adhesion, and antibacterial properties and promotes osteoblast differentiation of Ti species [202, 223], pristine CNTs are reported to increase oxidative stress and cause cell death [202].

In the example of Ag–MWCNTs coating, the mechanisms of antibacterial activity slightly differ depending on the form of silver, either ionic Ag^+ cations or NPs [153, 224, 225]. Both silver forms specifically interact with bacteria. For Ag NPs, the contact mechanism is typical which occurs through the touch of bacteria to silver particulates and ROS appearance, which leads to damage to the cell membrane and vacuolization of cytoplasm [226–230]. According to [231], all contacted Ag NPs influence the permeability and flow through the outer membrane, but only smaller Ag NPs can pass through the cell membrane, then interact with DNA, and affect the respiratory system. Whereas, the antibacterial mechanism for Ag^+ starts with their adhesion to the bacteria cell, its adsorption inside the bacteria cell, and the production of ROS [226, 228, 229, 232]. As Zhao et al. propose [230], the silver ions on the cell membrane inhibit the expression of outer membrane proteins, i.e., retard the reproduction of bacteria cells by inducing the release of nucleic acids, what is according to Du et al. [232] typical of large agglomerates of Ag NPs. The synergy of the combination of CNTs with Ag enhances the bactericidal efficiency of the CNTs, thus the Ag NPs are characterized by a high surface-to-volume ratio and MWCNTs high aspect ratio, this way produce a higher contact area [199]. Figure 8 schematically illustrates the differences in antibacterial mechanisms of CNTs and CNTs with Ag addition.

4.8 Perspectives and challanges

The CNTs gain more and more attention in biomedical, energy and thermal applications due to its excellent properties, such as crack bridging, increase in elastic modulus, improvement of thermal conductivity and heat transfer, and lubricating effect, which lowers the friction coefficient and improves wear resistance of coatings composed of CNTs. What is more, the CNTs addition generally improves the corrosion resistance of coatings by sealing pores, increases coating adhesion strength, due to the formation of a network in the coating and has antibacterial properties, especially against gram-negative bacteria. In endoprosthesis applications, Young's modulus near the cortical bone (of 15–30 GPa [233]), reported in [142] causes the MWCNTs coatings to be a suitable candidate for biomedical applications. Besides medical applications, the most promising perspectives for nanocarbon can be considered for the production of advanced, highly anticorrosive and self-repairing coatings [16], for green energy applications [234], for electronic and photonics [235].

Although there are many reports analyzing the properties of various CNTs coatings and composites, there are still several challenges and further questions to answer. The first one is the cytotoxicity issue of CNTs. Even if the studies demonstrate a general role of increasing the cytotoxicity of CNTs a high dose of CNTs in the coating, the smallest diameter, and the longer length of CNTs, the impact of functionalization on cytotoxic activity is still not enough known. The functionalization of CNTs enables its solubility, its deposition via electrochemical methods, thus the charged particles are required in this group of methods to prepare the coating, but there are also reports about its impact on decreasing the CNTs cytotoxicity [188–192], which still should be an open question to scientists.

Also, the adhesion mechanism of the CNTs coatings is a challenge to discuss. Up to now the adhesion of CNTs to some substrate occurs probably due to physical contact or weak van der Waals interaction, when describing coatings deposited electrochemically or by thermal sprayed methods. Nevertheless, the knowledge of CNTs adhesion mechanisms might be valuable when creating the solution for the problem with improvement of the adhesion strength of CNTs, which is also still challenging.

The same question might be posed on the subject of the bioactivity mechanism of CNTs, which is connected with the functionalization and adhesion strength of the CNTs-containing coating. The CNTs functionalization has an impact on coating surface architecture and thus cell adhesion, while the poor adhesion strength might be the reason for the excessive release of toxic substances in the human body.

The least but not last challenge for CNTs coatings is an improvement of its antibacterial properties against gram-positive bacteria. The gram-negative bacteria are protected by a narrow membrane, thus it is easier to break it and cause bacteria cell leakage, while gram-positive bacteria have up to 10 times thicker peptidoglycan walls and for, e.g., *B. subtilis* has peritrichous flagella structures which have smooth structure, so are unfavorable substrate for CNTs adhesion [198].

This review is a summary of coating properties composed of CNTs and different metals, ceramics and polymers, deposited on different substrates. The development of CNTs coatings still needs more research.

5 Conclusions

The state-of-the-art in the carbon nanotubes field shows a huge amount of research performed on CNTs coatings. The different forms of CNTs, deposition methods, and parameters, and substrates were applied as process variables. The microstructures, chemical and phase compositions, mechanical properties at the micro and nanoscale such as coating Young`s modulus and hardness, interface adhesion strength and delaminating force, open corrosion potential and corrosion current density, contact angle in wettability assessment, and bioactivity, cytotoxicity, and antibacterial efficiency among biological properties were determined. The following conclusions demonstrating valuable results and their implications, and still observed inefficiencies, can be drawn:

1. The MWCNTs are the most frequently and promising carbon nanoforms presumably because of the highest strength and the lowest Young`s modulus which is important for the mechanical behavior of coatings on artificial implants.
2. There is a diversity of deposition techniques applied for CNTs-containing coatings, all relatively similarly used, a choice of which depends on the expected properties and destination of the coated substrate.
3. Electrophoretic deposition is widely used for titanium and its alloys at the most preferred voltage of 5–30 V, time 0.5–5 min.
4. The roughness is the most plausible for biological application by coatings obtained by EPD, 0.2–1.0 µm, and the roughness of coatings prepared by thermal spray and plasma electrochemical oxidation seems excessive, 4–20 µm.
5. The shear strength test seems the most used technique to assess the adhesion which ranges between 15 and 35 MPa. The nanoindentation scratch technique seems the most precise for a great number of softer coatings, but it urgently needs to be quantified and standardized.
6. Hardness and Young`s modulus are measured by microhardness and nanoindentation tests and their values vary in wide limits depending on the substrate and phase and microstructure of a coating. The best hardness values reach 19 and 32 MPa for pure CNTs and CNTs strengthened with YSZ on steel substrate, relatively, and the lowest Young`s modulus is observed for the softer coatings on titanium and its alloys, 3–15 GPa. The use of either micro or nanohardness testing depends on the presumed toughness of a coating, and in such coatings is not highly accurate as evidenced by high values of standard deviations as compared to means.
7. Corrosion current density is only determined by potentiodynamic technique, and the obtained values range between some or tens of µA/cm^2. The corrosion resistance can presumably increase with a fraction of CNTs due to increasing inhomogeneity of coatings, still, however, remaining in a low corrosion rate area. The highest corrosion resistivity was observed for coatings with 1 wt% of CNTs.
8. The coatings CNTs-containing are hydrophilic, but their increasing content seems to lead toward higher contact angles. Such an effect might be expected for carbon nanoforms and likely can disappear after proper CNTs` functionalization.
9. The CNTs promote bioactivity assessed by the deposition of bone-like phosphates. However, the cytotoxicity of coatings implemented with long and narrow carbon nanotubes can be toxic, and this problem needs further thorough studies.

10. The coatings based on the CNTs show significant killing properties against the number of various bacteria, including the most dangerous encountered in hospitals.
11. Further research on the design and deposition of CNTs-including coatings is desired, in particular, to improve the adhesion of CNTs and the other components or a substrate, optimization of hardness and elasticity of coatings, and an assessment of relationships between cytotoxicity, functionalization, and content of CNTs in the coating.

Declarations

Conflict of interest The authors declare that they have no conflicts of interest.

References

1. Hopley EL, Salmasi S, Kalaskar DM, Seifalian AM (2014) Carbon nanotubes leading the way forward in new generation 3D tissue engineering. Biotechnol Adv 32:1000–1014. https://doi.org/10.1016/j.biotechadv.2014.05.003
2. Rathinavel S, Priyadharshini K, Panda D (2021) A review on carbon nanotube: an overview of synthesis, properties, functionalization, characterization, and the application. Mater Sci Eng B 268:115095. https://doi.org/10.1016/j.mseb.2021.115095
3. Iijima S (1991) Helical microtubules of graphitic carbon. Nature 354:56–58. https://doi.org/10.1038/354056a0
4. Thostenson ET, Ren Z, Chou T-W (2001) Advances in the science and technology of carbon nanotubes and their composites: a review. Compos Sci Technol 61:1899–1912. https://doi.org/10.1016/S0266-3538(01)00094-X
5. Khaniki HB, Ghayesh MH (2020) A review on the mechanics of carbon nanotube strengthened deformable structures. Eng Struct 220:110711. https://doi.org/10.1016/j.engstruct.2020.110711
6. Mousavi SR, Estaji S, Kiaei H et al (2022) A review of electrical and thermal conductivities of epoxy resin systems reinforced with carbon nanotubes and graphene-based nanoparticles. Polym Test 112:107645. https://doi.org/10.1016/j.polymertesting.2022.107645
7. Souto LFC, Henriques RR, Soares BG (2022) Influence of acidic and alkaline environmental anticorrosive performance of epoxy coatings based on polyaniline/carbon nanotube hybrids modified with ionic liquid. Prog Org Coat 173:107206. https://doi.org/10.1016/j.porgcoat.2022.107206
8. Li X, Wang J, Tian Y et al (2022) Thermal enhancement by constructing ordered-orienting hybrid network with modified boron nitride, graphene and carbon nanotubes in epoxy composite coatings. Prog Org Coat. https://doi.org/10.1016/j.porgcoat.2022.107078
9. Han W, Zhou J, Shi Q (2023) Research progress on enhancement mechanism and mechanical properties of FRP composites reinforced with graphene and carbon nanotubes. Alex Eng J 64:541–579. https://doi.org/10.1016/j.aej.2022.09.019
10. Qi X, Yang J, Zhang N et al (2021) Selective localization of carbon nanotubes and its effect on the structure and properties of polymer blends. Prog Polym Sci 123:101471. https://doi.org/10.1016/j.progpolymsci.2021.101471
11. Soni SK, Thomas B, Swain A, Roy T (2022) Functionally graded carbon nanotubes reinforced composite structures: an extensive review. Compos Struct 299:116075. https://doi.org/10.1016/j.compstruct.2022.116075
12. Deng H, Sheng L, Zhao X et al (2022) Non-noble metal FeMn and single-walled carbon nanotubes nanocomposites as effective bifunctional electrocatalysts in alkaline media for oxygen/hydrogen revolution reactions. Chin J Anal Chem 50:100110. https://doi.org/10.1016/j.cjac.2022.100110
13. Lee J, Kyeong D, Kim J, Choi W (2022) Layer-by-layer self-assembled functional coatings of carbon nanotube-polyethylenimine for enhanced heat transfer of heat sinks. Int J Heat Mass Transf. https://doi.org/10.1016/j.ijheatmasstransfer.2021.122344
14. Xia Y, Zhang S, Tong L et al (2022) Introducing cyano-functionalized multiwalled carbon nanotubes to improve corrosion resistance and mechanical performance of poly(arylene ether nitrile) coating. Surf Coat Technol 432:128058. https://doi.org/10.1016/j.surfcoat.2021.128058
15. Mao T, Li C, Mao F et al (2022) A durable anti-corrosion superhydrophobic coating based on carbon nanotubes and SiO2 aerogel for superior protection for Q235 steel. Diam Relat Mater 129:109370. https://doi.org/10.1016/j.diamond.2022.109370
16. Hosseinpour A, Rezaei Abadchi M, Mirzaee M, Tabar FA, Ramezanzadeh B (2021) Recent advances and future perspectives for carbon nanostructures reinforced organic coating for anti-corrosion application. Surf Interfaces 23:100994. https://doi.org/10.1016/j.surfin.2021.100994
17. Yan D, Zhang Z, Zhang W et al (2022) Smart self-healing coating based on the highly dispersed silica/carbon nanotube nanomaterial for corrosion protection of steel. Prog Org Coat 164:106694. https://doi.org/10.1016/j.porgcoat.2021.106694
18. Islam A, Pandey KK, Singh P et al (2022) Microstructural, mechanical and tribological properties of carbon nanotubes reinforced plasma sprayed molybdenum disulphide composite coatings. Ceram Int 48:32757–32766. https://doi.org/10.1016/j.ceramint.2022.07.200
19. Han B, Chen Y, Tan C et al (2022) Microstructure and wear behavior of laser clad interstitial CoCrFeNi high entropy alloy coating reinforced by carbon nanotubes. Surf Coat Technol 434:128241. https://doi.org/10.1016/j.surfcoat.2022.128241
20. Gu Y, Ma L, Yan M et al (2022) Strategies for improving friction behavior based on carbon nanotube additive materials. Tribol Int 176:107875. https://doi.org/10.1016/j.triboint.2022.107875
21. Zhu Z, Kang S, Chen H et al (2022) Construction of superhydrophobic alkyl siloxane-modified carbon nanotubes/epoxy coating. Diam Relat Mater 129:109351. https://doi.org/10.1016/j.diamond.2022.109351
22. Ma Y, Zhang J, Zhu G et al (2022) Robust photothermal self-healing superhydrophobic coating based on carbon nanosphere/carbon nanotube composite. Mater Des 221:110897. https://doi.org/10.1016/j.matdes.2022.110897
23. Zhang X, Mo Z, Arenal R et al (2023) Efficient oil-water separation by a robust superhydrophobic coating prepared directly

from commercial lacquer using silanized multi-walled carbon nanotubes as filler. Appl Surf Sci 609:155208. https://doi.org/10.1016/j.apsusc.2022.155208
24. Liu Y, Shao Y, Wang Y, Wang J (2022) An abrasion-resistant, photothermal, superhydrophobic anti-icing coating prepared by polysiloxane-modified carbon nanotubes and fluorine-silicone resin. Colloids Surf A 648:129335. https://doi.org/10.1016/j.colsurfa.2022.129335
25. Liu N, Guo L, Kou G et al (2022) Carbon nanotube reinforced pyrocarbon matrix composites with high coefficient of thermal expansion for self-adapting ultra-high-temperature ceramic coatings. Ceram Int 48:15668–15676. https://doi.org/10.1016/j.ceramint.2022.02.101
26. Hu L, Kang Z (2021) Enhanced flexible polypropylene fabric with silver/magnetic carbon nanotubes coatings for electromagnetic interference shielding. Appl Surf Sci 568:150845. https://doi.org/10.1016/j.apsusc.2021.150845
27. Chen C, Xiao G, Zhong F et al (2022) Synergistic effect of carbon nanotubes bonded graphene oxide to enhance the flame retardant performance of waterborne intumescent epoxy coatings. Prog Org Coat 162:106598. https://doi.org/10.1016/j.porgcoat.2021.106598
28. Chen C, Xiao G, Zhong F et al (2022) Dendritic-hydroxyzinc stannate loaded carbon nanotubes for enhancing flame retardancy of composite coatings. Colloids Surf A Physicochem Eng Asp 648:129329. https://doi.org/10.1016/j.colsurfa.2022.129329
29. Zhan W, Ni L, Gu Z et al (2021) The influences of graphene and carbon nanotubes on properties of waterborne intumescent fire resistive coating. Powder Technol 385:572–579. https://doi.org/10.1016/j.powtec.2021.03.018
30. Agasti N, Gautam V, Priyanka N et al (2022) Carbon nanotube based magnetic composites for decontamination of organic chemical pollutants in water: a review. Appl Surf Sci Adv 10:100270. https://doi.org/10.1016/j.apsadv.2022.100270
31. Lin WT, Lin ZW, Kuo TY et al (2022) Mechanical and biological properties of atmospheric plasma-sprayed carbon nanotube-reinforced tantalum pentoxide composite coatings on Ti6Al4V alloy. Surf Coat Technol 437:128356. https://doi.org/10.1016/j.surfcoat.2022.128356
32. Cha JH, Jang WH, Noh JE et al (2022) A space stealth and cosmic radiation shielding composite: polydopamine-coating and multi-walled carbon nanotube grafting onto an ultra-high-molecular-weight polyethylene/hydrogen-rich benzoxazine composite. Compos Sci Technol 230:109711. https://doi.org/10.1016/j.compscitech.2022.109711
33. Wang F, Zhao S, Jiang Q et al (2022) Advanced functional carbon nanotube fibers from preparation to application. Cell Rep Phys Sci 3:100989. https://doi.org/10.1016/j.xcrp.2022.100989
34. Dong Z, Sun B, Zhu H et al (2021) A review of aligned carbon nanotube arrays and carbon/carbon composites: fabrication, thermal conduction properties and applications in thermal management. New Carbon Mater 36:873–892. https://doi.org/10.1016/S1872-5805(21)60090-2
35. Shahzad N, Lutfullah PT et al (2022) Counter electrode materials based on carbon nanotubes for dye-sensitized solar cells. Renew Sustain Energy Rev 159:112196. https://doi.org/10.1016/j.rser.2022.112196
36. Xia Y, Zhu X, Qiu P et al (2022) Nano-confinement coating strategy derived Matryoshka-like carbon nanotubes@anatase nanocrystalline@amorphous carbon nanofibers for ultrafast sodium ion storage. Electrochim Acta 428:140941. https://doi.org/10.1016/j.electacta.2022.140941
37. Zakaria MR, Omar MF, Zainol Abidin MS et al (2022) Recent progress in the three-dimensional structure of graphene-carbon nanotubes hybrid and their supercapacitor and high-performance battery applications. Compos Part 154:106756. https://doi.org/10.1016/j.compositesa.2021.106756
38. Khan N, Han G, Mazari SA (2022) Carbon nanotubes-based anode materials for potassium ion batteries: a review. J Electroanal Chem 907:116051. https://doi.org/10.1016/j.jelechem.2022.116051
39. Jyoti J, Gupta TK, Singh BP et al (2022) Recent advancement in three dimensional graphene-carbon nanotubes hybrid materials for energy storage and conversion applications. J Energy Storage 50:104235. https://doi.org/10.1016/j.est.2022.104235
40. Afsarimanesh N, Nag A, Eshrat e Alahi M et al (2022) A critical review of the recent progress on carbon nanotubes-based nanogenerators. Sens Actuators A 344:113743. https://doi.org/10.1016/j.sna.2022.113743
41. Tran PA, Zhang L, Webster TJ (2009) Carbon nanofibers and carbon nanotubes in regenerative medicine. Adv Drug Deliv Rev 61:1097–1114. https://doi.org/10.1016/j.addr.2009.07.010
42. Raphey VR, Henna TK, Nivitha KP et al (2019) Advanced biomedical applications of carbon nanotube. Mater Sci Eng C 100:616–630. https://doi.org/10.1016/j.msec.2019.03.043
43. Liu X, Miller AL, Park S et al (2017) Functionalized carbon nanotube and graphene oxide embedded electrically conductive hydrogel synergistically stimulates nerve cell differentiation. ACS Appl Mater Interfaces 9:14677–14690. https://doi.org/10.1021/acsami.7b02072
44. Xiang C, Zhang Y, Guo W, Liang X-J (2020) Biomimetic carbon nanotubes for neurological disease therapeutics as inherent medication. Acta Pharm Sin B 10:239–248. https://doi.org/10.1016/j.apsb.2019.11.003
45. Mezzasalma SA, Grassi L, Grassi M (2021) Physical and chemical properties of carbon nanotubes in view of mechanistic neuroscience investigations Some outlook from condensed matter, materials science and physical chemistry. Mater Sci Eng C 131:112480. https://doi.org/10.1016/j.msec.2021.112480
46. Sebaa M, Nguyen TY, Paul RK et al (2013) Graphene and carbon nanotube–graphene hybrid nanomaterials for human embryonic stem cell culture. Mater Lett 92:122–125. https://doi.org/10.1016/j.matlet.2012.10.035
47. Foldvari M, Bagonluri M (2008) Carbon nanotubes as functional excipients for nanomedicines: I. pharmaceutical properties. Nanomedicine 4:173–182. https://doi.org/10.1016/j.nano.2008.04.002
48. Murjani BO, Kadu PS, Bansod M et al (2022) Carbon nanotubes in biomedical applications: current status, promises, and challenges. Carbon Lett 32:1207–1226. https://doi.org/10.1007/s42823-022-00364-4
49. Anzar N, Hasan R, Tyagi M et al (2020) Carbon nanotube—a review on Synthesis, Properties and plethora of applications in the field of biomedical science. Sens Int 1:100003. https://doi.org/10.1016/j.sintl.2020.100003
50. Kravanja KA, Finšgar M (2022) A review of techniques for the application of bioactive coatings on metal-based implants to achieve controlled release of active ingredients. Mater Des 217:110653. https://doi.org/10.1016/j.matdes.2022.110653
51. Bjelić D, Finšgar M (2022) Bioactive coatings with anti-osteoclast therapeutic agents for bone implants: enhanced compliance and prolonged implant life. Pharmacol Res 176:106060. https://doi.org/10.1016/j.phrs.2022.106060
52. Zhao X, Chang S, Long J et al (2019) The toxicity of multi-walled carbon nanotubes (MWCNTs) to human endothelial cells: the influence of diameters of MWCNTs. Food Chem Toxicol 126:169–177. https://doi.org/10.1016/j.fct.2019.02.026
53. Barrejón M, Marchesan S, Alegret N, Prato M (2021) Carbon nanotubes for cardiac tissue regeneration: state of the art and

perspectives. Carbon 184:641–650. https://doi.org/10.1016/j.carbon.2021.08.059
54. Arumugam S, Ju Y (2021) Carbon nanotubes reinforced with natural/synthetic polymers to mimic the extracellular matrices of bone—a review. Mater Today Chem 20:100420. https://doi.org/10.1016/j.mtchem.2020.100420
55. Zieliński A, Majkowska-Marzec B (2022) Whether carbon nanotubes are capable, promising, and safe for their application in nervous system regeneration. Some critical remarks and research strategies. Coatings 12:1643. https://doi.org/10.3390/coatings12111643
56. Teixeira-Santos R, Gomes M, Gomes LC, Mergulhão FJ (2021) Antimicrobial and anti-adhesive properties of carbon nanotube-based surfaces for medical applications: a systematic review. iScience 24:102001. https://doi.org/10.1016/j.isci.2020.102001
57. Horandghadim N, Ghazanfar-Ahari Y, Khalil-Allafi J (2022) Multiwalled-carbon nanotubes reinforced hydroxyapatite-tantalum pentoxide nanocomposite coating on Nitinol alloy: antibacterial activity and Electrochemical properties. Surf Interfaces 29:101773. https://doi.org/10.1016/j.surfin.2022.101773
58. Hadzhieva Z, Boccaccini AR (2022) Recent developments in electrophoretic deposition (EPD) of antibacterial coatings for biomedical applications—a review. Curr Opin Biomed Eng 21:100367. https://doi.org/10.1016/j.cobme.2021.100367
59. Dai B, Zhou R, Ping J et al (2022) Recent advances in carbon nanotube-based biosensors for biomolecular detection. TrAC Trends Anal Chem 154:116658. https://doi.org/10.1016/j.trac.2022.116658
60. Hurt RH, Monthioux M, Kane A (2006) Toxicology of carbon nanomaterials: status, trends, and perspectives on the special issue. Carbon 44:1028–1033. https://doi.org/10.1016/j.carbon.2005.12.023
61. Alshehri R, Ilyas AM, Hasan A et al (2016) Carbon nanotubes in biomedical applications: factors, mechanisms, and remedies of toxicity. J Med Chem 59:8149–8167. https://doi.org/10.1021/acs.jmedchem.5b01770
62. Kong H, Wang L, Zhu Y et al (2015) Culture medium-associated physicochemical insights on the cytotoxicity of carbon nanomaterials. Chem Res Toxicol 28:290–295. https://doi.org/10.1021/tx500477y
63. Kobayashi N, Izumi H, Morimoto Y (2017) Review of toxicity studies of carbon nanotubes. J Occup Health 59:394–407. https://doi.org/10.1539/joh.17-0089-RA
64. Gaillard C, Cellot G, Li S et al (2009) Carbon nanotubes carrying cell-adhesion peptides do not interfere with neuronal functionality. Adv Mater 21:2903–2908. https://doi.org/10.1002/adma.200900050
65. Abousalman-Rezvani Z, Eskandari P, Roghani-Mamaqani H, Salami-Kalajahi M (2020) Functionalization of carbon nanotubes by combination of controlled radical polymerization and "grafting to" method. Adv Colloid Interface Sci 278:102126. https://doi.org/10.1016/j.cis.2020.102126
66. Eskandari P, Abousalman-Rezvani Z, Roghani-Mamaqani H, Salami-Kalajahi M (2021) Polymer-functionalization of carbon nanotube by in situ conventional and controlled radical polymerizations. Adv Colloid Interface Sci 294:102471. https://doi.org/10.1016/j.cis.2021.102471
67. Hosseini H, Ghaffarzadeh M (2022) Surface functionalization of carbon nanotubes via plasma discharge: a review. Inorg Chem Commun 138:109276. https://doi.org/10.1016/j.inoche.2022.109276
68. Lavagna L, Nisticò R, Musso S, Pavese M (2021) Functionalization as a way to enhance dispersion of carbon nanotubes in matrices: a review. Mater Today Chem 20:100477. https://doi.org/10.1016/j.mtchem.2021.100477
69. Klein KL, Melechko AV, McKnight TE et al (2008) Surface characterization and functionalization of carbon nanofibers. J Appl Phys 103:061301. https://doi.org/10.1063/1.2840049
70. Asghar F, Murtaza B, Shakoor B et al (2022) Properties, assembly and characterization of carbon nanotubes: their application in water purification, environmental pollution control and biomedicines—a comprehensive review. Carbon Lett 33:275–306. https://doi.org/10.1007/s42823-022-00432-9
71. Banhart F (2020) Elemental carbon in the sp1 hybridization. ChemTexts 6:3. https://doi.org/10.1007/s40828-019-0098-z
72. Eatemadi A, Daraee H, Karimkhanloo H et al (2014) Carbon nanotubes: properties, synthesis, purification, and medical applications. Nanoscale Res Lett 9:393. https://doi.org/10.1186/1556-276X-9-393
73. Guler O, Bagci N (2020) A short review on mechanical properties of graphene reinforced metal matrix composites. J Mater Res Technol 9:6808–6833. https://doi.org/10.1016/J.JMRT.2020.01.077
74. Choudhary V, Gupt A (2011) Polymer/carbon nanotube nanocomposites. In: Silva Y (ed) Carbon nanotubes—polymer nanocomposites. InTech, pp 65–90. ISBN: 978-953-307-498-6. http://www.intechopen.com/books/carbon-nanotubes-polymer-nanocomposites/polymer-carbon-nanotube-nanocomposites. Accessed Sept 2023
75. Cai Shen H, Brozena A, Wang YuHuang (2011) Double-walled carbon nanotubes: challenges and opportunities. Nanoscale 3:503–518. https://doi.org/10.1039/C0NR00620C
76. Fonseca A, Hernadi K, Piedigrosso P et al (1998) Synthesis of single- and multi-wall carbon nanotubes over supported catalysts. Appl Phys A 67:11–22. https://doi.org/10.1007/S003390050732
77. Kang J, Al-Sabah S, Théo R (2020) Effect of single-walled carbon nanotubes on strength properties of cement composites. Materials 13:1305. https://doi.org/10.3390/ma13061305
78. Hussain A, Liao Y, Zhang Q et al (2018) Floating catalyst CVD synthesis of single walled carbon nanotubes from ethylene for high performance transparent electrodes. Nanoscale 10:9752–9759. https://doi.org/10.1039/C8NR00716K
79. Liu Y, Qian W, Zhang Q et al (2008) The confined growth of double-walled carbon nanotubes in porous catalysts by chemical vapor deposition. Carbon 46:1860–1868. https://doi.org/10.1016/j.carbon.2008.07.040
80. He M, Magnin Y, Amara H et al (2017) Linking growth mode to lengths of single-walled carbon nanotubes. Carbon 113:231–236. https://doi.org/10.1016/j.carbon.2016.11.057
81. Saito Y, Nakahira T, Uemura S (2003) Growth conditions of double-walled carbon nanotubes in arc discharge. J Phys Chem B 107:931–934. https://doi.org/10.1021/jp021367o
82. Rashad AA, Abd S, Mohammed A et al (2016) Synthesis of carbon nanotube: a review. J Nanosci Technol 2:155–162
83. Choudhary V, Singh BP, Mathur RB (2013) Carbon nanotubes and their composites. In: Satoru S (ed) Syntheses and applications of carbon nanotubes and their composites. InTech, pp 193–222. https://doi.org/10.5772/52897 (**ISBN: 978-953-51-1125-2**)
84. Doh J, Lee J (2016) Prediction of the mechanical behavior of double walled-CNTs using a molecular mechanics-based finite element method: Effects of chirality. Comput Struct 169:91–100. https://doi.org/10.1016/j.compstruc.2016.03.006
85. Kumar R, Singh RK, Ghosh AK et al (2013) Synthesis of coal-derived single-walled carbon nanotube from coal by varying the ratio of Zr/Ni as bimetallic catalyst. J Nanopart Res 15:1406. https://doi.org/10.1007/s11051-012-1406-3
86. Tian Y, Zhang Y, Wang B et al (2004) Coal-derived carbon nanotubes by thermal plasma jet. Carbon 42:2597–2601. https://doi.org/10.1016/j.carbon.2004.05.042

87. Hoang VC, Hassan M, Gomes VG (2018) Coal derived carbon nanomaterials—recent advances in synthesis and applications. Appl Mater Today 12:342–358. https://doi.org/10.1016/j.apmt.2018.06.007
88. Dorfman MR (2018) Thermal spray coatings. In: Myer K (ed) Handbook of environmental degradation of materials, 3rd edn. Elsevier, New York, pp 469–488. https://doi.org/10.1016/B978-0-323-52472-8.00023-X
89. Vuoristo P (2014) Thermal spray coating processes. In: Saleem H, Gilmar FB, Chester JVT, Bekir Y (eds) Comprehensive materials processing. Elsevier, Woodhead Publishing, New York, pp 229–276. https://doi.org/10.1016/B978-0-08-096532-1.00407-6
90. Venturi F, Kamnis S, Hussain T (2021) Internal diameter HVOAF thermal spray of carbon nanotubes reinforced WC-Co composite coatings. Mater Des 202:109566. https://doi.org/10.1016/j.matdes.2021.109566
91. Lombardi AN, Casteletti LC, Totten GE (2013) Thermal spray technologies: an overview. In: Wang QJ, Chung YW (eds) Encyclopedia of tribology. Springer, US, Boston, pp 3607–3617. https://doi.org/10.1007/978-0-387-92897-5_684
92. Makhlouf ASH (2011) Current and advanced coating technologies for industrial applications. In: Abdel SHM, Ion T (eds) Nanocoatings and ultra-thin films. Elsevier, Woodhead Publishing, New York, pp 3–23. https://doi.org/10.1533/9780857094902.1.3
93. Wang M (2010) Composite coatings for implants and tissue engineering scaffolds. In: Luigi A (ed) Biomedical composites. Elsevier, Woodhead Publishing Series in Biomaterials, New York, pp 127–177. https://doi.org/10.1533/9781845697372.2.127
94. He P, Wang H, Chen S et al (2020) Interface characterization and scratch resistance of plasma sprayed TiO_2-CNTs nanocomposite coating. J Alloys Compd 819:153009. https://doi.org/10.1016/j.jallcom.2019.153009
95. Xie X, Tan Z, Chen C et al (2021) Synthesis of carbon nanotube reinforced Al matrix composite coatings via cold spray deposition. Surf Coat Technol 405:126676. https://doi.org/10.1016/j.surfcoat.2020.126676
96. Assadi H, Gärtner F, Stoltenhoff T, Kreye H (2003) Bonding mechanism in cold gas spraying. Acta Mater 51:4379–4394. https://doi.org/10.1016/S1359-6454(03)00274-X
97. Basha GMT, Bolleddu V (2021) Tribological behavior of carbon nanotubes reinforced high velocity oxy-fuel sprayed WC-20 wt% Co coatings. J Therm Spray Technol 30:1653–1665. https://doi.org/10.1007/s11666-021-01230-x
98. Li M, Christofides PD (2009) Modeling and control of high-velocity oxygen-fuel (HVOF) thermal spray: a tutorial review. J Therm Spray Technol 18:753–768. https://doi.org/10.1007/s11666-009-9309-2
99. Tucker RC (1995) Plasma spray, detonation gun, and HVOF deposition techniques. In: Yves P (ed) Materials and processes for surface and interface engineering, NATO ASI series, vol 290. Springer, Dordrecht, pp 245–284. https://doi.org/10.1007/978-94-011-0077-9_7
100. Murray JW, Rance GA, Xu F, Hussain T (2018) Alumina-graphene nanocomposite coatings fabricated by suspension high velocity oxy-fuel thermal spraying for ultra-low-wear. J Eur Ceram Soc 38:1819–1828. https://doi.org/10.1016/j.jeurceramsoc.2017.10.022
101. Mishra NK, Mishra SB (2015) Hot corrosion performance of LVOF sprayed Al_2O_3–40% TiO_2 coating on Superni 601 and Superco 605 superalloys at 800 and 900 °C. Bull Mater Sci 38:1679–1685. https://doi.org/10.1007/s12034-015-0986-9
102. Moonngam S, Tunjina P, Deesom D, Banjongprasert C (2016) Fe-Cr/CNTs nanocomposite feedstock powders produced by chemical vapor deposition for thermal spray coatings. Surf Coat Technol 306:323–327. https://doi.org/10.1016/j.surfcoat.2016.07.024
103. Huang Y, Zhu L, Huang Q, He Z (2022) The light absorption enhancement of nanostructured carbon-based coatings fabricated by high-voltage electrostatic spraying technique. Opt Mater (Amst) 133:112902. https://doi.org/10.1016/j.optmat.2022.112902
104. Quintino L (2014) Overview of coating technologies. In: Miranda R (ed) Surface modification by solid state processing. Elsevier, Woodhead Publishing, New York, pp 1–24. https://doi.org/10.1533/9780857094698.1
105. Shivamurthy RC, Kamaraj M, Nagarajan R, Shariff SM, Padmanabham G (2012) Laser surface modification of steel for slurry erosion resistance in power plants. In: Kwok CT (ed) Laser surface modification of alloys for corrosion and erosion resistance. In Woodhead Publishing series in metals and surface engineering. Elsevier, New York, pp 177–287. https://doi.org/10.1533/9780857095831.2.177
106. Yuan W, Li R, Chen Z et al (2021) A comparative study on microstructure and properties of traditional laser cladding and high-speed laser cladding of Ni45 alloy coatings. Surf Coat Technol 405:126582. https://doi.org/10.1016/j.surfcoat.2020.126582
107. Zhang Y, Wang Q, Ye R, Ramachandran CS (2022) Plasma electrolytic oxidation of cold spray kinetically metallized CNT-Al coating on AZ91-Mg alloy: evaluation of mechanical and surficial characteristics. J Alloys Compd 892:162094. https://doi.org/10.1016/j.jallcom.2021.162094
108. Xie X, Chen C, Ji G, Xu R, Tan Z, Xie Y, Li Z, Liao H (2019) A novel approach for fabricating a CNT/AlSi composite with the self-aligned nacre-like architecture by cold spraying. Nano Mater Sci 1:137–141. https://doi.org/10.1016/j.nanoms.2019.04.002
109. Joshi B, Samuel E, Kim Y, Yarin AL, Swihart MT, Yoon SS (2021) Electrostatically sprayed nanostructured electrodes for energy conversion and storage devices. Adv Funct Mater 31:2008181. https://doi.org/10.1002/adfm.202008181
110. Li G, Feng L, Tong P, Zhai Z (2016) The properties of MWCNT/polyurethane conductive composite coating prepared by electrostatic spraying. Prog Org Coat 90:284–290. https://doi.org/10.1016/j.porgcoat.2015.10.018
111. Rogala-Wielgus D, Majkowska-Marzec B, Zieliński A et al (2021) Mechanical behavior of bi-layer and dispersion coatings composed of several nanostructures on Ti13Nb13Zr alloy. Materials 14:2905. https://doi.org/10.3390/ma14112905
112. Majkowska-Marzec B, Tęczar P, Bartmański M et al (2020) Mechanical and corrosion properties of laser surface-treated Ti13Nb13Zr alloy with MWCNTs coatings. Materials 13:3991. https://doi.org/10.3390/ma13183991
113. Khalili V, Khalil-Allafi J, Maleki-Ghaleh H, Paulsen A, Frenzel J, Eggeler G (2016) The influence of Si as reactive bonding agent in the electrophoretic coatings of HA–Si–MWCNTs on NiTi alloys. J Mater Eng Perform 25:390–400. https://doi.org/10.1007/s11665-015-1824-3
114. Bordbar M, Alimohammadi T, Khoshnevisan B, Khodadadi B, Yeganeh-Faal A (2015) Preparation of MWCNT/TiO_2 –Co nanocomposite electrode by electrophoretic deposition and electrochemical study of hydrogen storage. Int J Hydrogen Energy 40:9613–9620. https://doi.org/10.1016/j.ijhydene.2015.05.138
115. Chávez-Valdez A, Boccaccini AR (2012) Innovations in electrophoretic deposition: alternating current and pulsed direct current methods. Electrochim Acta 65:70–89. https://doi.org/10.1016/j.electacta.2012.01.015
116. Dicu MM, Balteanu AM (2021) Coating techniques for materials medical: a mini-review. In: Proceedings of the 13th international conference on electronics, computers and artificial intelligence,

ECAI 2021. Institute of Electrical and Electronics Engineers Inc, pp: 1–5. https://doi.org/10.1109/ECAI52376.2021.9515152
117. Abdel-Karim R (2016) Electrochemical synthesis of nanocomposites. In: Mohamed AMA, Golden TD (eds) Electrodeposition of composite materials. InTech. https://doi.org/10.5772/62189 (**ISBN: 978-953-51-2270-8**)
118. Azmi AA, Jai J, Zamanhuri NA, Yahya A (2018) Precious metals recovery from electroplating wastewater: a review. IOP Conf Ser Mater Sci Eng 358:012024. https://doi.org/10.1088/1757-899X/358/1/012024
119. Yuan W, Li R, Zhu Y et al (2022) Structure and properties of nickel-plated CNTs/Fe-based amorphous composite coatings fabricated by high-speed laser cladding. Surf Coat Technol 438:128363. https://doi.org/10.1016/j.surfcoat.2022.128363
120. Li QH, Savalani MM, Zhang QM, Huo L (2014) High temperature wear characteristics of TiC composite coatings formed by laser cladding with CNT additives. Surf Coat Technol 239:206–211. https://doi.org/10.1016/j.surfcoat.2013.11.043
121. Zhai L, Ban C, Zhang J, Yao X (2019) Characteristics of dilution and microstructure in laser cladding Ni-Cr-B-Si coating assisted by electromagnetic compound field. Mater Lett 243:195–198. https://doi.org/10.1016/j.matlet.2019.01.133
122. Liu J, Sun W, Huang Y (2021) Effect of carbon nanotubes content on microstructure and properties of WC/Ni laser cladding coatings. Surf Eng 37:650–657. https://doi.org/10.1080/02670844.2020.1812481
123. Bakshi SR, Singh V, Seal S, Agarwal A (2009) Aluminum composite reinforced with multiwalled carbon nanotubes from plasma spraying of spray dried powders. Surf Coat Technol 203:1544–1554. https://doi.org/10.1016/j.surfcoat.2008.12.004
124. Bakshi SR, Keshri AK, Agarwal A (2011) A comparison of mechanical and wear properties of plasma sprayed carbon nanotube reinforced aluminum composites at nano and macro scale. Mater Sci Eng A 528:3375–3384. https://doi.org/10.1016/j.msea.2011.01.061
125. Abdulameer S, Al-Sultani KF, Majdi HS (2022) MWCNTS-YSZ coating deposited by plasma thermal spray on ICONEL 738 low carbon substrate. Mater Today Proc 60:1241–1247. https://doi.org/10.1016/j.matpr.2021.08.144
126. Yu L, Jia P, Song Y et al (2022) Effect of carbon nanotubes on the microstructure and properties of plasma electrolytic oxidized ceramic coatings on high silicon aluminum alloy. J Mater Res Technol 18:3541–3552. https://doi.org/10.1016/j.jmrt.2022.04.035
127. Thakare JG, Mulik RS, Mahapatra MM (2018) Effect of carbon nanotubes and aluminum oxide on the properties of a plasma sprayed thermal barrier coating. Ceram Int 44:438–451. https://doi.org/10.1016/j.ceramint.2017.09.196
128. Daram P, Banjongprasert C, Thongsuwan W, Jiansirisomboon S (2016) Microstructure and photocatalytic activities of thermal sprayed titanium dioxide/carbon nanotubes composite coatings. Surf Coat Technol 306:290–294. https://doi.org/10.1016/j.surfcoat.2016.06.068
129. Mohammed Thalib Basha G, Srikanth A, Venkateshwarlu B (2020) Effect of reinforcement of carbon nanotubes on air plasma sprayed conventional Al_2O_3–3%TiO_2 ceramic coatings. Mater Today Proc 20:191–194. https://doi.org/10.1016/J.MATPR.2019.11.025
130. Zhang Y, Wang Q, Chen G, Ramachandran CS (2020) Mechanical, tribological and corrosion physiognomies of CNT-Al metal matrix composite (MMC) coatings deposited by cold gas dynamic spray (CGDS) process. Surf Coat Technol 403:126380. https://doi.org/10.1016/j.surfcoat.2020.126380
131. Pialago EJT, Kwon OK, Park CW (2013) Nucleate boiling heat transfer of R134a on cold sprayed CNT–Cu composite coatings. Appl Therm Eng 56:112–119. https://doi.org/10.1016/j.applthermaleng.2013.03.046
132. Pialago EJT, Kwon OK, Kim M-S, Park CW (2015) Ternary Cu–CNT–AlN composite coatings consolidated by cold spray deposition of mechanically alloyed powders. J Alloys Compd 650:199–209. https://doi.org/10.1016/j.jallcom.2015.08.007
133. Pialago EJT, Kwon OK, Jin JS, Park CW (2016) Nucleate pool boiling of R134a on cold sprayed Cu–CNT–SiC and Cu–CNT–AlN composite coatings. Appl Therm Eng 103:684–694. https://doi.org/10.1016/j.applthermaleng.2016.04.022
134. Ye Z, Li J, Liu L et al (2021) Microstructure and wear performance enhancement of carbon nanotubes reinforced composite coatings fabricated by laser cladding on titanium alloy. Opt Laser Technol 139:106957. https://doi.org/10.1016/j.optlastec.2021.106957
135. Pialago EJT, Yoo J, Zheng X, Zhenga X, Kima BR, Honga SJ, Kwonb OK, Park CW (2020) Experimental investigation of the heat transfer performance of capillary-assisted horizontal evaporator tubes with sintered porous hydrophilic copper-carbon nanotube-titanium dioxide (Cu–CNT–TiO_2) composite coatings for adsorption chiller. Int J Heat Mass Transf 147:118958. https://doi.org/10.1016/j.ijheatmasstransfer.2019.118958
136. Tripathi P, Katiyar PK, Ramkumar J, Balani K (2020) Synergistic role of carbon nanotube and yttria stabilised zirconia reinforcement on wear and corrosion resistance of Cr-based nano-composite coatings. Surf Coat Technol 385:125381. https://doi.org/10.1016/j.surfcoat.2020.125381
137. Shukla P, Awasthi S, Ramkumar J, Balani K (2018) Protective trivalent Cr-based electrochemical coatings for gun barrels. J Alloys Compd 768:1039–1048. https://doi.org/10.1016/j.jallcom.2018.07.170
138. Suzuki T, Konno T (2014) Improvement in tool life of electroplated diamond tools by Ni-based carbon nanotube composite coatings. Precis Eng 38:659–665. https://doi.org/10.1016/j.precisioneng.2014.03.003
139. Deesom D, Charoenrut K, Moonngam S, Banjongprasert C (2016) Fabrication and properties of NiCr/CNTs nanocomposite coatings prepared by High Velocity Oxy-Fuel Spraying. Surf Coat Technol 306:240–244. https://doi.org/10.1016/j.surfcoat.2016.06.016
140. Dlugon E, Simka W, Fraczek-Szczypta A, Niemiec W, Markowski J, Szymanska M, Blazewicz M (2015) Carbon nanotube-based coatings on titanium. Bull Mater Sci 38:1339–1344. https://doi.org/10.1007/s12034-015-1019-4
141. Singh I, Allan P, London W (2007) Nano-mechanical testing of novel bioactive carbon nanotubes/HAP nano particles composite coating. NSTI Nanotech 4:145–148
142. Majkowska-Marzec B, Rogala-Wielgus D, Bartmański M et al (2019) Comparison of properties of the hybrid and bilayer MWCNTs—hydroxyapatite coatings on Ti Alloy. Coatings 9:643. https://doi.org/10.3390/coatings9100643
143. Rogala-Wielgus D, Majkowska-Marzec B, Zieliński A, Jankiewicz BJ (2021) Mechanical behavior of bi-layer and dispersion coatings composed of several nanostructures on Ti substrate. Appl Sci 11:7862. https://doi.org/10.3390/app11177862
144. Xu L, Wang J, Wu R, Wang J, Wu H, Li Y, Hou L, Zhang J (2021) Microstructure and mechanical properties of Mg-14Li-1Al/MWCNTs composites prepared by electrophoretic deposition and accumulative roll bonding. J Manuf Process 72:431–438. https://doi.org/10.1016/j.jmapro.2021.10.040
145. Maleki-Ghaleh H, Khalil-Allafi J (2019) Effect of hydroxyapatite-titanium-MWCNTs composite coating fabricated by electrophoretic deposition on corrosion and cellular behavior of NiTi alloy. Mater Corr 70:2128–2138. https://doi.org/10.1002/maco.201910940

146. Zhu QG, Sujari ANA, Ab Ghani S (2012) Electrophoretic deposited MWCNT composite graphite pencils and its uses to determine hyperin. J Solid State Electrochem 16:3179–3187. https://doi.org/10.1007/s10008-012-1749-9
147. Majkowska-Marzec B, Sypniewska J (2021) Microstructure and mechanical properties of laser surface-treated Ti13Nb13Zr alloy with MWCNTs coatings. Adv Mater Sci 21:5–18. https://doi.org/10.2478/adms-2021-0021
148. Nguyen TT, Pham NT, Dinh TTM, Vu TT, Nguyen HS, Tran LD (2020) Electrodeposition of hydroxyapatite-multiwalled carbon nanotube nanocomposite on Ti6Al4V. Adv Polym Technol 2020:1–10. https://doi.org/10.1155/2020/8639687
149. Sundaram RM, Sekiguchi A, Sekiya M et al (2018) Copper/carbon nanotube composites: research trends and outlook. R Soc Open Sci 5:180814. https://doi.org/10.1098/rsos.180814
150. Datta M (2009) Electrodeposition. In: Shacham-Diamand Y, Osaka T, Datta M, Ohba T (eds) Advanced nanoscale ULSI interconnects: fundamentals and applications. Springer, New York, pp 63–71. https://doi.org/10.1007/978-0-387-95868-2_4
151. Nasirpouri F, Yousefi I, Moslehifard E, Khalil-Allafi J (2017) Tuning surface morphology and crystallinity of anodic TiO_2 nanotubes and their response to biomimetic bone growth for implant applications. Surf Coat Technol 315:163–171. https://doi.org/10.1016/j.surfcoat.2017.02.006
152. Yang Y, Yu M, Böke F, Qina Q, Hübnerc R, Knusta S, Schwidereka S, Grundmeiera G, Fischerb H, Keller A (2021) Effect of nanoscale surface topography on the adsorption of globular proteins. Appl Surf Sci 535:147671. https://doi.org/10.1016/j.apsusc.2020.147671
153. Yang C, Jian R, Huang K, Wang Q, Feng B (2021) Antibacterial mechanism for inactivation of *E. coli* by AgNPs@polydoamine/titania nanotubes via speciation analysis of silver ions and silver nanoparticles by cation exchange reaction. Microchem J 160:105636. https://doi.org/10.1016/j.microc.2020.105636
154. Li N, Sun S, Bai H, Xu W, Xiao G, Zhang Y, Lu Y (2020) Evolution of nano/submicro-scale oxide structures on Ti6Al4V achieved by an ultrasonic shot peening-induction heating approach for high-performance surface design of bone implants. J Alloys Compd 831:154876. https://doi.org/10.1016/j.jallcom.2020.154876
155. Elias CN, Fernandes DJ, Resende CRS, Roestel J (2015) Mechanical properties, surface morphology and stability of a modified commercially pure high strength titanium alloy for dental implants. Dent Mater 31:e1–e13. https://doi.org/10.1016/j.dental.2014.10.002
156. Lee Y, Jung A, Heo S-J, Gweona B, Lim D (2023) Influences of surface topography of porous titanium scaffolds manufactured by powder bed fusion on osteogenesis. J Mater Res Technol 23:2784–2797. https://doi.org/10.1016/j.jmrt.2023.01.153
157. Alhmoud H, Brodoceanu D, Elnathan R, Kraus T, Voelcker NH (2021) A MACEing silicon: towards single-step etching of defined porous nanostructures for biomedicine. Prog Mater Sci 116:100636. https://doi.org/10.1016/j.pmatsci.2019.100636
158. Schlie S, Fadeeva E, Koroleva A, Ovsianikov A, Koch J, Ngezahayo A, Chichkov BN (2011) Laser-based nanoengineering of surface topographies for biomedical applications. Photonics Nanostruct 9:159–162. https://doi.org/10.1016/j.photonics.2010.09.006
159. Yazdani J, Ahmadian E, Sharifi S, Shahib S, Dizaj SM (2018) A short view on nanohydroxyapatite as coating of dental implants. Biomed Pharmacother 105:553–557. https://doi.org/10.1016/j.biopha.2018.06.013
160. Sonamuthu J, Samayanan S, Jeyaraman AR, Murugesana B, Krishnana B, Mahalingam S (2018) Influences of ionic liquid and temperature on the tailorable surface morphology of F-apatite nanocomposites for enhancing biological abilities for orthopedic implantation. Mater Sci Eng C 84:99–107. https://doi.org/10.1016/j.msec.2017.11.035
161. Kryszak B, Szustakiewicz K, Dzienny P, Junka K, Paleczny J, Szymczyk-Ziółkowska P, Hoppe V, Antończak A (2022) Functionalization of the PLLA surface with a femtosecond laser: tailored substrate properties for cellular response. Polym Test 116:107815. https://doi.org/10.1016/j.polymertesting.2022.107815
162. Hasturk O, Ermis M, Demirci U, Hasirci N, Hasirci V (2019) Square prism micropillars on poly(methyl methacrylate) surfaces modulate the morphology and differentiation of human dental pulp mesenchymal stem cells. Colloids Surf B Biointerfaces 178:44–55. https://doi.org/10.1016/j.colsurfb.2019.02.037
163. Goldbaum D, Shockley JM, Chromik RR, Rezaeian A, Yue S, Legoux JG, Irissou E (2012) The effect of deposition conditions on adhesion strength of Ti and Ti6Al4V cold spray splats. J Therm Spray Technol 21:288–303. https://doi.org/10.1007/s11666-011-9720-3
164. Brohede U, Zhao S, Lindberg F, Mihranyan A, Forsgren J, Strømme M, Engqvist H (2009) A novel graded bioactive high adhesion implant coating. Appl Surf Sci 255:7723–7728. https://doi.org/10.1016/j.apsusc.2009.04.149
165. Mohseni E, Zalnezhad E, Bushroa AR (2014) Comparative investigation on the adhesion of hydroxyapatite coating on Ti–6Al–4V implant: a review paper. Int J Adhes Adhes 48:238–257. https://doi.org/10.1016/j.ijadhadh.2013.09.030
166. Alkhodary MA (2023) Effect of controlled surface roughness and biomimetic coating on titanium implants adhesion to the bone: an experiment animal study. Saudi Dent J. https://doi.org/10.1016/j.sdentj.2023.07.010
167. Lin C, Han H, Zhang F, Li A (2008) Electrophoretic deposition of HA/MWNTs composite coating for biomaterial applications. J Mater Sci Mater Med 19:2569–2574. https://doi.org/10.1007/s10856-007-3196-1
168. Gopi D, Shinyjoy E, Sekar M, Surendiran M, Kavitha L, Kumar TSS (2013) Development of carbon nanotubes reinforced hydroxyapatite composite coatings on titanium by electrodeposition method. Corros Sci 73:321–330. https://doi.org/10.1016/j.corsci.2013.04.021
169. Pei X, Zeng Y, He R, Li Z, Tian L, Wang J, Wan Q, Li X, Bao H (2014) Single-walled carbon nanotubes/hydroxyapatite coatings on titanium obtained by electrochemical deposition. Appl Surf Sci 295:71–80. https://doi.org/10.1016/j.apsusc.2014.01.009
170. Maleki-Ghaleh H, Khalil-Allafi J (2019) Characterization, mechanical and in vitro biological behavior of hydroxyapatite-titanium-carbon nanotube composite coatings deposited on NiTi alloy by electrophoretic deposition. Surf Coat Technol 363:179–190. https://doi.org/10.1016/j.surfcoat.2019.02.029
171. Zhong Z, Qin J, Ma J (2015) Electrophoretic deposition of biomimetic zinc substituted hydroxyapatite coatings with chitosan and carbon nanotubes on titanium. Ceram Int 41:8878–8884. https://doi.org/10.1016/j.ceramint.2015.03.145
172. Yi C, Bagchi S, Dmuchowski CM, Gou F, Chen X, Park C, Chew HB, Ke C (2018) Direct nanomechanical characterization of carbon nanotubes—titanium interfaces. Carbon 132:548–555. https://doi.org/10.1016/j.carbon.2018.02.069
173. Yi C, Chen X, Gou F, Dmuchowski CM, Sharma A, Park C, Ke C (2017) Direct measurements of the mechanical strength of carbon nanotube—aluminum interfaces. Carbon 125:93–102. https://doi.org/10.1016/j.carbon.2017.09.020
174. Kaya C, Kaya F, Cho J, Roether JA, Boccaccini AR (2009) Carbon nanotube-reinforced hydroxyapatite coatings on metallic implants using electrophoretic deposition. Key Eng Mater 412:93–97. https://doi.org/10.4028/www.scientific.net/KEM.412.93

175. Lahiri D, Ghosh S, Agarwal A (2012) Carbon nanotube reinforced hydroxyapatite composite for orthopedic application: a review. Mater Sci Eng C 32:1727–1758. https://doi.org/10.1016/j.msec.2012.05.010
176. Heary RF, Parvathreddy N, Sampath S, Agarwal N (2017) Elastic modulus in the selection of interbody implants. J Spine Surg 3:163–167. https://doi.org/10.21037/jss.2017.05.01
177. Pawłowski Ł, Rościszewska M, Majkowska-Marzec B et al (2022) Influence of surface modification of titanium and its alloys for medical implants on their corrosion behavior. Materials 15:7556. https://doi.org/10.3390/ma15217556
178. Heise S, Forster C, Heer S, Qi H, Zhou J, Virtanen S, Lu T, Boccaccini AR (2019) Electrophoretic deposition of gelatine nanoparticle/chitosan coatings. Electrochim Acta 307:318–325. https://doi.org/10.1016/j.electacta.2019.03.145
179. Fujita K, Obara S, Maru J, Endoh S (2020) Cytotoxicity profiles of multi-walled carbon nanotubes with different physico-chemical properties. Toxicol Mech Methods 30:477–489. https://doi.org/10.1080/15376516.2020.1761920
180. Nagai H, Okazaki Y, Chew SH et al (2011) Diameter and rigidity of multiwalled carbon nanotubes are critical factors in mesothelial injury and carcinogenesis. Proc Natl Acad Sci 108:E1330–E1338. https://doi.org/10.1073/pnas.1110013108
181. Long J, Xiao Y, Liu L, Cao Y (2017) The adverse vascular effects of multi-walled carbon nanotubes (MWCNTs) to human vein endothelial cells (HUVECs) in vitro: role of length of MWCNTs. J Nanobiotechnol 15:80. https://doi.org/10.1186/s12951-017-0318-x
182. Dinç B, Ünlü A, Bektaş M (2020) Characterization of short-length multi-walled carbon nanotubes and cytotoxicity on MDA-MB-231 and HUVEC cell lines. Carbon Lett 30:143–153. https://doi.org/10.1007/s42823-019-00081-5
183. Sun Y, Gong J, Cao Y (2019) Multi-walled carbon nanotubes (MWCNTs) activate apoptotic pathway through ER stress: does surface chemistry matter? Int J Nanomed 14:9285–9294. https://doi.org/10.2147/IJN.S217977
184. Shende P, Augustine S, Prabhakar B (2020) A review on graphene nanoribbons for advanced biomedical applications. Carbon Lett 30:465–475. https://doi.org/10.1007/s42823-020-00125-1
185. Pietroiusti A, Massimiani M, Fenoglio I et al (2011) Low doses of pristine and oxidized single-wall carbon nanotubes affect mammalian embryonic development. ACS Nano 5:4624–4633. https://doi.org/10.1021/nn200372g
186. Thakur A, Bharti R, Sharma R (2022) Carbon nanotubes: types, synthesis, cytotoxicity and applications in biomedical. Mater Today Proc 50:2256–2268. https://doi.org/10.1016/j.matpr.2021.10.002
187. Zhao X, Lu D, Hao F, Liu R (2015) Exploring the diameter and surface dependent conformational changes in carbon nanotube-protein corona and the related cytotoxicity. J Hazard Mater 292:98–107. https://doi.org/10.1016/j.jhazmat.2015.03.023
188. Lu N, Sui Y, Ding Y, Tian R, Li L, Liu F (2018) Adsorption of human serum albumin on functionalized single-walled carbon nanotubes reduced cytotoxicity. Chem Biol Interact 295:64–72. https://doi.org/10.1016/j.cbi.2018.03.015
189. Ding Y, Tian R, Yang Z, Chen J, Lu N (2017) Effects of serum albumin on the degradation and cytotoxicity of single-walled carbon nanotubes. Biophys Chem 222:1–6. https://doi.org/10.1016/j.bpc.2016.12.002
190. Tian R, Long X, Yang Z, Lu N, Peng YY (2020) Formation of a bovine serum albumin diligand complex with rutin and single-walled carbon nanotubes for the reduction of cytotoxicity. Biophys Chem 256:106268. https://doi.org/10.1016/j.bpc.2019.106268
191. Aghaleh M, Rafiee A, Morowvat MH, Ghasemi Y (2021) Evaluating the cytotoxicity of single-walled and multi-walled carbon nanotubes as a scaffold for human chondrocyte stem cell precursors and optimizing the operational conditions. Mater Today Commun 29:102979. https://doi.org/10.1016/j.mtcomm.2021.102979
192. Alam AKMM, Beg MDH, Yunus RM, Islam MR, Shubhra QTH (2021) Tailoring the dispersibility of non-covalent functionalized multi-walled carbon nanotube (MWCNT) nanosuspension using shellac (SL) bio-resin: structure-property relationship and cytotoxicity of shellac coated carbon nanotubes (SLCNTs). Colloid Interface Sci Commun 42:100395. https://doi.org/10.1016/j.colcom.2021.100395
193. Xia Y, Li S, Nie C et al (2019) A multivalent polyanion-dispersed carbon nanotube toward highly bioactive nanostructured fibrous stem cell scaffolds. Appl Mater Today 16:518–528. https://doi.org/10.1016/j.apmt.2019.07.006
194. Gao C, Feng P, Peng S, Shuai C (2017) Carbon nanotube, graphene and boron nitride nanotube reinforced bioactive ceramics for bone repair. Acta Biomater 61:1–20. https://doi.org/10.1016/j.actbio.2017.05.020
195. Misra SK, Ohashi F, Valappil SP et al (2010) Characterization of carbon nanotube (MWCNT) containing P(3HB)/bioactive glass composites for tissue engineering applications. Acta Biomater 6:735–742. https://doi.org/10.1016/j.actbio.2009.09.023
196. Stango AX, Vijayalakshmi U (2018) Electrochemically grown functionalized-multi-walled carbon nanotubes/hydroxyapatite hybrids on surgical grade 316L SS with enhanced corrosion resistance and bioactivity. Colloids Surf B Biointerfaces 171:186–196. https://doi.org/10.1016/j.colsurfb.2018.06.058
197. Seo S-J, Kim J-J, Kim J-H, Lee JY, Shin US, Li EJ, Kim HW (2014) Enhanced mechanical properties and bone bioactivity of chitosan/silica membrane by functionalized-carbon nanotube incorporation. Compos Sci Technol 96:31–37. https://doi.org/10.1016/j.compscitech.2014.03.004
198. Liu S, Ng AK, Xu R, Wei J, Tan CM, Yang Y, Chen Y (2010) Antibacterial action of dispersed single-walled carbon nanotubes on *Escherichia coli* and *Bacillus subtilis* investigated by atomic force microscopy. Nanoscale 2:2744–2750. https://doi.org/10.1039/c0nr00441c
199. Dinh NX, Van QN, Huy TQ, Le AT (2015) Decoration of silver nanoparticles on multiwalled carbon nanotubes: antibacterial mechanism and ultrastructural analysis. J Nanomater 2015:1–11. https://doi.org/10.1155/2015/814379
200. Schifano E, Cavoto G, Pandolfi F et al (2023) Plasma-etched vertically aligned CNTs with enhanced antibacterial power. Nanomaterials 13:1081. https://doi.org/10.3390/nano13061081
201. Rajavel K, Gomathi R, Manian S, Rajendra Kumar RT (2014) In vitro bacterial cytotoxicity of CNTS: reactive oxygen species mediate cell damage edges over direct physical puncturing. Langmuir 30:592–601. https://doi.org/10.1021/la403332b
202. Zhu Y, Liu X, Yeung KWK, Yeung KWK, Chu PK, Wu S (2017) Biofunctionalization of carbon nanotubes/chitosan hybrids on Ti implants by atom layer deposited ZnO nanostructures. Appl Surf Sci 400:14–23. https://doi.org/10.1016/j.apsusc.2016.12.158
203. Jatoi AW, Ogasawara H, Kim IS, Ni Q-Q (2020) Cellulose acetate/multi-wall carbon nanotube/Ag nanofiber composite for antibacterial applications. Mater Sci Eng C 110:110679. https://doi.org/10.1016/j.msec.2020.110679
204. Yun H, Kim JD, Choi HC, Lee CW (2013) Antibacterial activity of CNT-Ag and GO-Ag nanocomposites against gram-negative and gram-positive bacteria. Bull Korean Chem Soc 34:3261–3264. https://doi.org/10.5012/bkcs.2013.34.11.3261
205. Baek S, Joo SH, Su C, Toborek M (2019) Antibacterial effects of graphene- and carbon-nanotube-based nanohybrids on *Escherichia coli*: implications for treating multidrug-resistant bacteria. J Environ Manag 247:214–223. https://doi.org/10.1016/j.jenvman.2019.06.077
206. Ma Y, Liu J, Yin H et al (2018) Remarkably improvement in antibacterial activity of carbon nanotubes by hybridizing with

silver nanodots. J Nanosci Nanotechnol 18:5704–5710. https://doi.org/10.1166/jnn.2018.15383
207. Zhao A, Zhang N, Li Q et al (2021) Incorporation of silver-embedded carbon nanotubes coated with tannic acid into polyamide reverse osmosis membranes toward high permeability, antifouling, and antibacterial properties. ACS Sustain Chem Eng 9:11388–11402. https://doi.org/10.1021/acssuschemeng.1c03313
208. Hamouda HI, Abdel-Ghafar HM, Mahmoud MHH (2021) Multi-walled carbon nanotubes decorated with silver nanoparticles for antimicrobial applications. J Environ Chem Eng 9:105034. https://doi.org/10.1016/j.jece.2021.105034
209. Kim JD, Yun H, Kim GC, Lee CW, Choi HC (2013) Antibacterial activity and reusability of CNT-Ag and GO-Ag nanocomposites. Appl Surf Sci 283:227–233. https://doi.org/10.1016/j.apsusc.2013.06.086
210. Xia L, Xu M, Cheng G et al (2018) Facile construction of Ag nanoparticles encapsulated into carbon nanotubes with robust antibacterial activity. Carbon 130:775–781. https://doi.org/10.1016/j.carbon.2018.01.073
211. Yin M, Huang D, Zhang X et al (2018) Preparation of Ag@CNT nanohybrids and investigations on their antibacterial and cytotoxicological effects. Nanosci Nanotechnol Lett 10:1671–1676. https://doi.org/10.1166/nnl.2018.2844
212. Gan L, Geng A, Jin L, Zhong Q, Wang L, Xu L, Mei C (2019) Antibacterial nanocomposite based on carbon nanotubes–silver nanoparticles-co-doped polylactic acid. Polymer Bull 77:793–804. https://doi.org/10.1007/S00289-019-02776-1
213. Joghataeian M, Bahari A, Qavami A, Raeisi MJ (2020) An antibacterial study of a new magnetic carbon nanotube/core-shell nanohybrids. J Environ Chem Eng 8:104150. https://doi.org/10.1016/j.jece.2020.104150
214. Khedaer Z, Ahmed D, Al-Jawad S (2021) Investigation of morphological, optical, and antibacterial properties of hybrid ZnO-MWCNT prepared by sol-gel. J Appl Sci Nanotechnol 1:66–77. https://doi.org/10.53293/jasn.2021.11634
215. Yazhini KB, Prabu HG (2014) Antibacterial activity of cotton coated with ZnO and ZnO-CNT composites. Appl Biochem Biotechnol 175:85–92. https://doi.org/10.1007/S12010-014-1257-8
216. Ding M, Sahebgharani N, Musharavati F, Jaber F, Zalnezhad E, Yoon GH (2018) Synthesis and properties of HA/ZnO/CNT nanocomposite. Ceram Int 44:7746–7753. https://doi.org/10.1016/j.ceramint.2018.01.203
217. Mohammad MR, Ahmed DS, Mohammed MKA (2019) Synthesis of Ag-doped TiO_2 nanoparticles coated with carbon nanotubes by the sol–gel method and their antibacterial activities. J Solgel Sci Technol 90:498–509. https://doi.org/10.1007/s10971-019-04973-w
218. Sukkar K, Duha SA, Hussein A, Mohammad RM (2019) Synthesis and characterization hybrid materials (TiO_2/MWCNTs) by chemical method and evaluating antibacterial activity against common microbial pathogens. Acta Phys Pol A 135:588–592. https://doi.org/10.12693/APhysPolA.135.588
219. Hossain MdA, Elias Md, Sarker DR et al (2018) Synthesis of Fe- or Ag-doped TiO_2–MWCNT nanocomposite thin films and their visible-light-induced catalysis of dye degradation and antibacterial activity. Res Chem Intermed 44:2667–2683. https://doi.org/10.1007/s11164-018-3253-z
220. Nguyen QX, Nguyen TT, Pham NM, Khong TT, Cao TM, Pham VV (2022) A fabrication of CNTs/TiO_2/polyurethane films toward antibacterial and protective coatings. Prog Org Coat 167:106838. https://doi.org/10.1016/j.porgcoat.2022.106838
221. Singh A, Goswami A, Nain S (2020) Enhanced antibacterial activity and photo-remediation of toxic dyes using Ag/SWCNT/PPy based nanocomposite with core–shell structure. Appl Nanosci 10:2255–2268. https://doi.org/10.1007/s13204-020-01394-y
222. Zhu Y, Xu J, Wang Y, Chen C, Gu H, Chai Y, Wang Y (2020) Silver nanoparticles-decorated and mesoporous silica coated single-walled carbon nanotubes with an enhanced antibacterial activity for killing drug-resistant bacteria. Nano Res 13:389–400. https://doi.org/10.1007/s12274-020-2621-3
223. Park JE, Park I-S, Neupane MP, Bae TS, Lee MH (2014) Effects of a carbon nanotube-collagen coating on a titanium surface on osteoblast growth. Appl Surf Sci 292:828–836. https://doi.org/10.1016/j.apsusc.2013.12.058
224. Li H, Gao Y, Li C, Ma G, Shang Y, Sun Y (2016) A comparative study of the antibacterial mechanisms of silver ion and silver nanoparticles by Fourier transform infrared spectroscopy. Vib Spectrosc 85:112–121. https://doi.org/10.1016/j.vibspec.2016.04.007
225. Wu Y, Yang Y, Zhang Z, Wang Z, Zhao Y, Sun L (2018) A facile method to prepare size-tunable silver nanoparticles and its antibacterial mechanism. Adv Powder Technol 29:407–415. https://doi.org/10.1016/j.apt.2017.11.028
226. Liu S, Zhang D, Chen W, Wang X, Ji H, Fu Y, Lü C (2023) Synthesis, antibacterial activity and action mechanism of silver-based nanomaterials with thermosensitive polymer-decorated graphene oxide as a stable support. Mater Today Commun 36:106598. https://doi.org/10.1016/j.mtcomm.2023.106598
227. Zhao Z, Li P, Xie R, Cao X, Su D, Shan Y (2022) Biosynthesis of silver nanoparticle composites based on hesperidin and pectin and their synergistic antibacterial mechanism. Int J Biol Macromol 214:220–229. https://doi.org/10.1016/j.ijbiomac.2022.06.048
228. Ji H, Zhou S, Fu Y, Wang Y, Mi J, Lu T, Wang X, Lü C (2020) Size-controllable preparation and antibacterial mechanism of thermo-responsive copolymer-stabilized silver nanoparticles with high antimicrobial activity. Mater Sci Eng C 110:110735. https://doi.org/10.1016/j.msec.2020.110735
229. Gallón SMN, Alpaslan E, Wang M et al (2019) Characterization and study of the antibacterial mechanisms of silver nanoparticles prepared with microalgal exopolysaccharides. Mater Sci Eng C 99:685–695. https://doi.org/10.1016/j.msec.2019.01.134
230. Zhao Y, Wee CY, Zhang H, Yang Z, Wang WEJ, Thian ES (2022) Silver-substituted hydroxyapatite inhibits *Pseudomonas aeruginosa* outer membrane protein F: a potential antibacterial mechanism. Biomater Adv 134:112713. https://doi.org/10.1016/j.msec.2022.112713
231. Jin Y, Zhu L, Xue W, Li W (2015) Fabrication of superaligned carbon nanotubes reinforced copper matrix laminar composite by electrodeposition. Trans Nonferrous Met Soc China 25:2994–3001. https://doi.org/10.1016/S1003-6326(15)63926-7
232. Du J, Hu Z, Dong W, Wang Y, Wu S, Bai Y (2019) Biosynthesis of large-sized silver nanoparticles using Angelica keiskei extract and its antibacterial activity and mechanisms investigation. Microchem J 147:333–338. https://doi.org/10.1016/j.microc.2019.03.046
233. Moghadasi K, Isa MSM, Ariffin MA et al (2022) A review on biomedical implant materials and the effect of friction stir based techniques on their mechanical and tribological properties. J Mater Res Technol 17:1054–1121
234. Ong YT, Ahmad AL, Zein SHS, Tan SH (2010) A review on carbon nanotubes in an environmental protection and green engineering perspective. Braz J Chem Eng 27:227–242
235. Kamanina N, Kuzhakov P, Kvashnin D (2020) Novel perspective coatings for the optoelectronic elements: features of the carbon nanotubes to modify the surface relief of BaF2 materials. Coatings 10:661. https://doi.org/10.3390/coatings10070661